A numerical study of the topology of hyperbolic manifolds supporting diffusion in a priori unstable systems.

Elena Lega, Massimiliano Guzzo, Claude Froeschle

A numerical study of the topology of hyperbolic manifolds supporting diffusion in a priori unstable systems.

Elena Lega
Observatoire de Nice, Bv. de l'Observatoire, B.P. 4229,
06304 Nice cedex 4, France.
Massimiliano Guzzo
Università degli Studi di Padova,
Dipartimento di Matematica Pura ed Applicata
via Trieste 63, 35121 Padova, Italy
Claude Froeschlé
Observatoire de Nice, Bv. de l'Observatoire, B.P. 4229,
06304 Nice cedex 4, France.

November 13, 2007

Abstract

Using new numerical methods we detect the topology of hyperbolic manifolds supporting diffusion in the a priori unstable dynamical systems and compare them with the diffusion properties. We measure a spread of the asymptotic manifolds which is significant to explain diffusion. We show that the stable and unstable manifolds have a topological transition when the Melnikov approximation looses its accuracy. This transition is correlated to a change of the law of dependence of the diffusion coefficient on the perturbing parameter. This suggests that the Melnikov approximation is not only a technical tool which allows one to compute accurate approximations of the manifolds at small values of the perturbing parameters, but is related to a dynamical regime.

1 Introduction

Diffusion in conservative dynamical systems has been a very studied subject in the last decades. Apart from specific examples, the understanding of the general mechanisms which can produce drift and

diffusion in the phase space of such systems is an interesting, and in general open, problem. In this paper we focus our attention on an important class of conservative systems, which we call *a priori unstable* ones following the terminology introduced in [4], while in a second paper [2] we consider the case of quasi–integrable systems.

Since the pioneering work of Arnold [1] many efforts have been done to relate diffusion in phase space to the topology of the so called stable and unstable manifolds of the normally hyperbolic invariant manifolds of the system. To fix ideas, we consider a discrete dynamical system defined by a symplectic map $\phi : M \to M$, M being a symplectic and Riemannian manifold, with a normally hyperbolic invariant manifold $\Lambda \subseteq M$ such that the dynamics of ϕ restricted to Λ has no diffusion, for example we require that any orbit of $\phi_{|\Lambda}$ is uniformly bounded by some constant c_0. It is interesting to study the diffusion in a neighborhood of Λ, that is, for any $c > c_0$ and $\rho > 0$ finding x, y up to a distance ρ from Λ which are on the same orbit and their distance is greater than c. In quasi–integrable systems this kind of diffusion is usually called Arnold diffusion, since Arnold's paper [1]. A way of proving the existence of this kind of diffusion is to prove that the stable and unstable manifolds of invariant objects of Λ intersect transversely. Precisely, for any $x_0, y_0 \in \Lambda$, one needs to prove that there exist $x_0, x_1, ..., x_N = y_0 \in \Lambda$ which belong to different invariant sets $A_0, A_1, ..., A_N \subseteq \Lambda$ such that the unstable manifold W_i^u of A_i and the stable manifold W_{i+1}^s of A_{i+1} intersect transversely. As a consequence, for any $\rho > 0$, there are points $\xi_0, ..., \xi_N$ within distance ρ from $x_0, ..., x_N$ which are on the same orbit. The sequence $x_0, ..., x_N$ is called transition chain, because the orbit which connects ξ_0, ξ_N passes through the neighborhoods of the points x_j. Therefore, this mechanism, which is called transition chain mechanism, provides a useful topological argument to prove the existence of 'some' specific orbits which diffuse in the phase–space, but it is not known up to now if it is the predominant mechanism of diffusion. The existence of the transition chain mechanism in a specific quasi–integrable system has been proved for the first time by Arnold, and up to now it has not been yet generalized to generic quasi–integrable Hamiltonian systems, while it has been proved very recently [6] for the so–called a priori unstable systems under quite general hypotheses. Independent proofs are published in [5] (based on Mather theory), in [21], [22] (based on the so called separatrix method).

One of the most important techniques to prove the existence of transitions chains (used in [6]) is the so–called Melnikov theory, which provides first order approximations of the stable and unstable manifolds.

In the last years we detected numerically diffusion in the Arnold web of quasi–integrable systems with a diffusion coefficient decreasing faster than a power law with respect to a perturbing parameter, which

we identified as Arnold diffusion [15], [17], [18]. Despite of the slowness of this diffusion, we were able to measure a statistical regularity in the diffusion properties of well chosen sets of initial conditions. For a priori unstable systems it is much simpler to detect sets of orbits which diffuse with a regular statistics (for a review see [16] and references therein). Can the transition chain mechanism explain these phenomena of regular diffusion of orbits?

In this paper we investigate numerically the topological properties of this kind of regular diffusion for the a priori unstable systems and we compare them with the transition chain mechanism. To do this, we use numerical methods to represent the stable and unstable manifolds of the 2–dimensional hyperbolic invariant manifolds embedded in a four dimensional space, using some methods which are based on existing ones and a new method which is based on the so called Fast Lyapunov Indicator (introduced in [11] and reviewed in the Appendix).

Our main result is the measure of a spread of the asymptotic stable (unstable) manifolds in the phase–space which is significant to explain diffusion. Given a generic point x in the invariant manifold, the dynamics maps all the points in a neighborhood U of x along the unstable manifold of x, and because of the spread of this unstable manifold, the set U spreads in the phase space and some of its points return near the invariant manifold 'far away' from the orbit of x. This is the mechanism that is behind the diffusion phenomena that we detect numerically.

In this sense, for generic diffusing orbits, we did not detect transitions from different stable and unstable manifolds, but this is likely due to the fact that the probability of finding an orbit which passes near selected number of heteroclinic points is very small.

The existence of heteroclinic transverse intersections remains a possible way to prove the spread of the asymptotic manifolds in certain situations, for example when the Melnikov approximation is valid.

At this regard, we show that the topology of the stable and unstable manifolds has a transition when the Melnikov approximation looses its accuracy. This transition is correlated to a change of the law of dependence of the diffusion coefficient on the perturbing parameter. This suggests that for these systems the Melnikov approximation is not only a technical tool which allows one to compute accurate approximations of the manifolds at small values of the perturbing parameters, but is related to a dynamical regime. We remark that such a transition, related to the Melnikov regime, occurs for values of the perturbing parameter which are smaller than the thresholds of transition to a Chirikov–like regime of global overlapping of resonances for the dynamics restricted to the normally hyperbolic invariant manifold.

The paper is organized as follows: in section 2 we recall some definitions about the normally hyperbolic invariant manifolds and we define our model example; in section 3 we recall the dynamical properties of a

priori–unstable systems which are useful in this paper; in section 4 we describe the numerical methods for detecting the structure of the stable (unstable) manifolds; in section 5 we report the results on the computation of the stable (unstable) manifolds and the comparison with the Melnikov approximation; in section 6 we connect the geometry of the manifolds to diffusion; in the appendix we review the fundamentals of the Fast Lyapunov Indicator method.

2 Hyperbolic invariant manifolds in a model problem

We investigate the diffusion properties of four dimensional symplectic maps near a normally hyperbolic invariant manifold. The notion of normally hyperbolic invariant manifolds was introduced in [3], and can be stated as follows (see, for example, [9]):

Definition ([3], [9]). *Let M be a $\mathcal{C}^q$ ($q \geq 1$) compact connected Riemannian manifold; let $U \subseteq M$ open and let $\phi : U \to M$ be a $\mathcal{C}^q$ embedding; let Λ be a sub-manifold of M which is invariant by ϕ. The map ϕ is said to be normally hyperbolic to Λ (Λ is also said to be normally hyperbolic invariant manifold) if for any point $x \in \Lambda$ the tangent space T_xM has the following splitting:*

$$T_xM = E^s(x) \oplus T_x\Lambda \oplus E^u(x)$$

which is invariant, i.e. the linear spaces $E^s(x), E^u(x)$ are invariant by ϕ:

$$D\phi E^s(x) \subseteq E^s(\phi(x)) \quad , \quad D\phi E^u(x) \subseteq E^u(\phi(x)) \quad ,$$

and there exist constants $\lambda_1, \lambda_2, \lambda_3, \mu_1, \mu_2, \mu_3$ satisfying:

$$0 < \lambda_1 \leq \mu_1 < \lambda_2 \leq \mu_2 < \lambda_3 \leq \mu_3 \quad , \quad \mu_1 < 1 < \lambda_3 \quad ,$$

such that:

$$\begin{aligned} \lambda_1 \leq \inf_{\xi \in E^s(x)\setminus 0} \frac{\|D\phi(x)\xi\|}{\|\xi\|} \leq \sup_{\xi \in E^s(x)\setminus 0} \frac{\|D\phi(x)\xi\|}{\|\xi\|} \leq \mu_1 \\ \lambda_2 \leq \inf_{\xi \in T_x\Lambda\setminus 0} \frac{\|D\phi(x)\xi\|}{\|\xi\|} \leq \sup_{\xi \in T_x\Lambda\setminus 0} \frac{\|D\phi(x)\xi\|}{\|\xi\|} \leq \mu_2 \\ \lambda_3 \leq \inf_{\xi \in E^u(x)\setminus 0} \frac{\|D\phi(x)\xi\|}{\|\xi\|} \leq \sup_{\xi \in E^u(x)\setminus 0} \frac{\|D\phi(x)\xi\|}{\|\xi\|} \leq \mu_3 \end{aligned} \quad . \quad (1)$$

The importance of normally hyperbolic invariant manifolds is mainly stated by the so called local stable (unstable) manifold theorem, which states the existence, at any $x \in \Lambda$ of the smooth manifolds $W_s^{loc}(x), W_u^{loc}(x)$ (see [3]) such that: $x \in W_s^{loc}(x), W_u^{loc}(x)$, $T_xW_s^{loc}(x) = E^s(x)$, $T_xW_u^{loc}(x) = E^u(x)$ and for any $n \geq 0$ it is:

$$y \in W_s^{loc}(x) \quad \Rightarrow \quad d(\phi^n(x), \phi^n(y)) \leq C(\mu_1 + c)^n d(x, y)$$

$$y \in W_u^{loc}(x) \quad \Rightarrow \quad d(\phi^{-n}(x), \phi^{-n}(y)) \leq C(\lambda_3 - c)^{-n} d(x, y)$$

with $C, c > 0$ suitable constants (c suitably small) and $d(\cdot, \cdot)$ denotes a distance on M. The manifolds $W_s(x), W_s(x)$ are then obtained by iterating the local manifolds $W_s^{loc}(x), W_u^{loc}(x)$ with ϕ^{-1} and ϕ respectively.

The local stable and unstable manifolds of Λ are defined by:

$$W_s^{loc} = \cup_{x \in \Lambda} W_s^{loc}(x) \quad , \quad W_u^{loc} = \cup_{x \in \Lambda} W_u^{loc}(x) \quad , \tag{2}$$

while the stable and unstable manifolds of Λ are:

$$W_s = \cup_{x \in \Lambda} W_s(x) \quad , \quad W_u = \cup_{x \in \Lambda} W_u(x) \quad , \tag{3}$$

Examples. The explicit examples given in this paper refer to the discrete system defined by the map:

$$\begin{array}{c} \phi : \mathbb{T}^4 \longrightarrow \mathbb{T}^4 \\ (\varphi_1, \varphi_2, I_1, I_2) \longmapsto (\varphi_1', \varphi_2', I_1', I_2') \end{array} \tag{4}$$

such that:

$$\begin{aligned} \varphi_1' &= \varphi_1 + I_1 \\ \varphi_2' &= \varphi_2 + I_2 \\ I_1' &= I_1 - a \sin \varphi_1' + \epsilon \frac{\sin \varphi_1'}{(\cos \varphi_1' + \cos \varphi_2' + c)^2} \\ I_2' &= I_2 + \epsilon \frac{\sin \varphi_2'}{(\cos \varphi_1' + \cos \varphi_2' + c)^2} \quad , \end{aligned} \tag{5}$$

where a, ϵ and $c > 2$ are parameters. The symplectic structure on $\mathbb{T}^4$ is $d\varphi_1 \wedge dI_1 + d\varphi_2 \wedge dI_2$. The map ϕ has the following invariant manifold:

$$\Lambda = \{(I_1, \varphi_1, I_2, \varphi_2) : \quad \text{such that} \quad (I_1, \varphi_1) = (0, \pi)\} \tag{6}$$

for any value of the parameters. In particular we will consider the following cases:

i) For $a > 0$ and $\epsilon = 0$ the manifold Λ is normally hyperbolic for a suitable choice of the Riemannian structure. For example, one can use the following flat norm of tangent vectors $\|(\xi_{\varphi_1}, \xi_{\varphi_2}, \xi_{I_1}, \xi_{I_2})\|^2 = |\xi_{\varphi_1}|^2 + \gamma |\xi_{\varphi_2}|^2 + |\xi_{I_1}|^2 + |\xi_{I_2}|^2$, with $\gamma \in (0, 1]$ suitably small. An alternative way to display the normal hyperbolicity of the map is to fix a Riemannian structure (for example with $\gamma = 1$) and then proving that ϕ^N is normally hyperbolic for some integer N.

The stable and unstable manifolds of Λ are the product of the stable and unstable manifolds of the hyperbolic fixed point of the standard map:

$$\varphi_1' = \varphi_1 + I_1 \quad , \quad I_1' = I_1 - a \sin \varphi_1'$$

with the torus $\mathbb{T}^2$, domain of (I_2, φ_2). Because normal hyperbolicity persists for small perturbations, Λ is normally hyperbolic also for suitably small ϵ. In this case the stable and unstable manifolds are not a product as in the previous case, and to describe their topology we will use Melnikov–like approximations and numerical techniques. The case $a > 0$ defines an a priori unstable system, because the invariant manifold Λ is hyperbolic also for $\epsilon = 0$.

ii) For $a = 0$, $\epsilon = 0$ the map is integrable and Λ is not hyperbolic. For $a = 0$ and $\epsilon \neq 0$ the map is quasi–integrable, the manifold Λ is still invariant (as well as the manifold $(I_2, \varphi_2) = (0, \pi)$), but one does not immediately recognize if it is hyperbolic. The diffusion in quasi–integrable systems at small values of the perturbing parameter is often called Arnold diffusion. Paper [2] is entirely dedicated to these systems.

3 Survey on the dynamics near hyperbolic invariant manifolds in the model problem

The dynamics of ϕ defined in (5) restricted to Λ has no diffusion if ϵ is suitably small. In fact, this dynamics is represented by the 2–dimensional map:

$$\varphi_2' = \varphi_2 + I_2 \quad , \quad I_2' = I_2 + \epsilon \frac{\sin \varphi_2'}{(\cos \varphi_2' + c - 1)^2} \quad , \tag{7}$$

whose invariant KAM curves bound any possibility of diffusion if ϵ is suitably small. Let us denote by ϵ_c the value such that KAM theorem is valid for any $0 < \epsilon \leq \epsilon_c$. As usual in KAM theory, the analytic estimate of ϵ_c can be inefficient, so that we refer to its numerical estimate obtained directly from the phase portraits of the restricted map. In figure 1 we report phase portraits of (7) obtained for different values of ϵ for $I_2 \in [0.26, 0.38]$. Approximately, for $\epsilon < 0.002$, the map has still many invariant tori which constitute a topological bound to chaotic diffusion. Instead, for $\epsilon = 0.0026$ the invariant tori seem to have disappeared, leaving the possibility to chaotic diffusion in the direction of the action I_2. Therefore, there is a numerical indication that $\epsilon_c \in (0.002, 0.0026)$ in this interval of the action. We recall that if the invariant tori are a topological barrier which completely stops diffusion, as soon as ϵ is bigger than ϵ_c there is the possibility of diffusion, but it can be very slow because of possible stickiness phenomena (see, for example, [8]) due to the presence of cantori and islands of regular motion [25]. These barriers to diffusion loose their effectiveness at higher values of ϵ. In this paper we are interested in the range $0 < \epsilon \leq \epsilon_c$, for which there is not diffusion on Λ and we study the diffusion properties

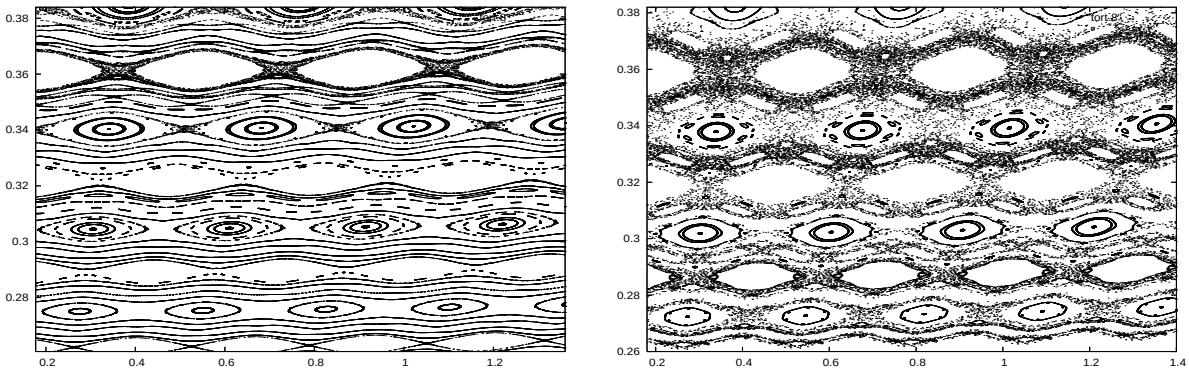

Figure 1: Phase portrait of the restricted map (7) for $\epsilon = 0.002, 0.0026$ and $c = 2.1$.

of a neighborhood of Λ. This can be done numerically by using the techniques which we used in [12], [15], [17], [18], [19] to study Arnold diffusion in quasi–integrable systems. Specifically:

i) individual orbits in a neighborhood of the invariant manifold indeed spread in the I_2 direction, as it is shown in figure 2.

ii) we measured the diffusion coefficient for $a = 0.4$, $c = 2.1$ for different values of ϵ for three sets of $N = 100$ initial conditions near $I_2 = 0.324$, $I_2 = 1.8$ and $I_2 = 2$ respectively (the other initial conditions are $I_1 \in [-10^{-5}, 10^{-5}]$, $\varphi_1 = \pi$, $\varphi_2 = 0$). More precisely, we computed the average evolution of the mean squared distance of a set of N orbits from their initial conditions. This quantity turns out to grow linearly with time, the slope giving the diffusion coefficient. The results, reported in figure 3, reveal that for the three sets the diffusion coefficient is well fitted by a power law $D(\epsilon) \simeq \epsilon^2$ for $\epsilon \leq 6\ 10^{-6}$. For $6\ 10^{-6} \leq \epsilon \leq 4\ 10^{-4}$ some irregularity can appear depending on the specific set of initial conditions, although data are not far from the $D(\epsilon) \simeq \epsilon^2$ law. For $\epsilon > 4\ 10^{-4}$ the power law changes to $D(\epsilon) \simeq \epsilon^{2.8}$. We anticipate (see section 5) that these changes in the law of dependence of D on ϵ seem to be correlated to changes in the topology of the stable (unstable) manifolds of Λ.

These experimental facts can be only partially explained by means of existing rigorous results. Precisely, though there does not exist in the literature a rigorous result proving diffusion of orbits for a system like (5), this system is very similar to those studied in [5], [21], [22], [6], for which diffusion of individual orbits is proved. The differences between the map (5) with $a \neq 0$ and the systems studied in those papers are: for $\epsilon = 0$ the system studied in [5], [21], [22], [6] is a simple pendulum

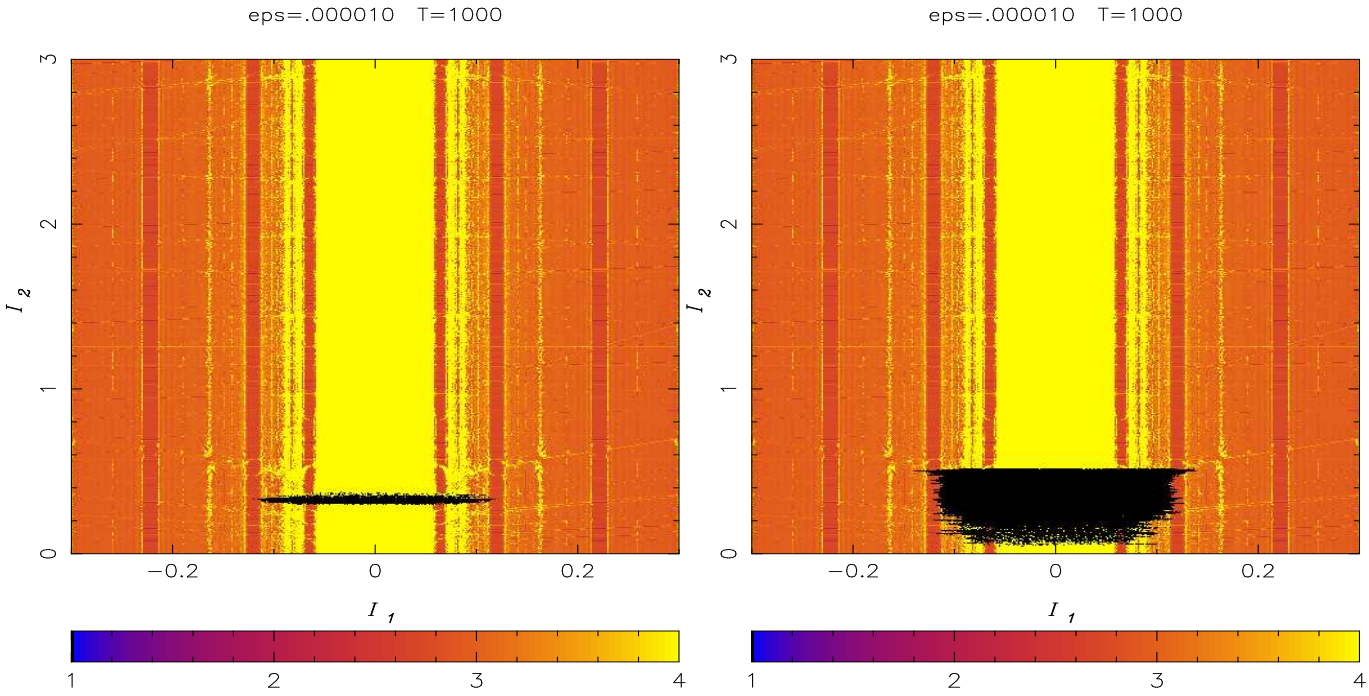

Figure 2: Representation of the FLI for the map (5) with $a = 0.4$, $c = 2.1$ and $\epsilon = 10^{-5}$. For any initial condition with $I_1 \in [-0.3, 0.3]$, $I_2 = [0, 3]$ we plot the value of the FLI after 1000 iterations of the map using a color scale. The black points on the FLI figure represent the points of the orbits of $N = 100$ initial conditions with $I_1 \in [-10^{-5}, 10^{-5}]$, $I_2 = 0.324$, $\varphi_1 = \pi$, $\varphi_2 = 0$ which re-enter in the neighborhood of the surface $S = \{(I_1, \varphi_1, I_2, \varphi_2)$ such that : $\varphi_1 = \pi \ , \ \varphi_2 = 0\}$ defined by $|\varphi_1 - \pi| + |\varphi_2| \leq 0.05$. In the left panel the orbits are computed up to 10^6 iterations, in the right panel up to 10^8 iterations.

coupled with a rotation (a more general case is considered in [21], [22], which includes perturbations of such a system), while for the map (5) the unperturbed case corresponds to a standard map coupled with a rotation. However, in both cases there is an invariant manifold which is hyperbolic also at $\epsilon = 0$; the dynamics on this invariant manifold can be represented by a 2D quasi–integrable map. As a consequence, the mechanism of transition introduced in [6] which takes into account the stable and unstable manifolds of all type of orbits (not only the invariant tori) could be important also in the present case. The techniques used in [6] are essentially based on the Melnikov approximation

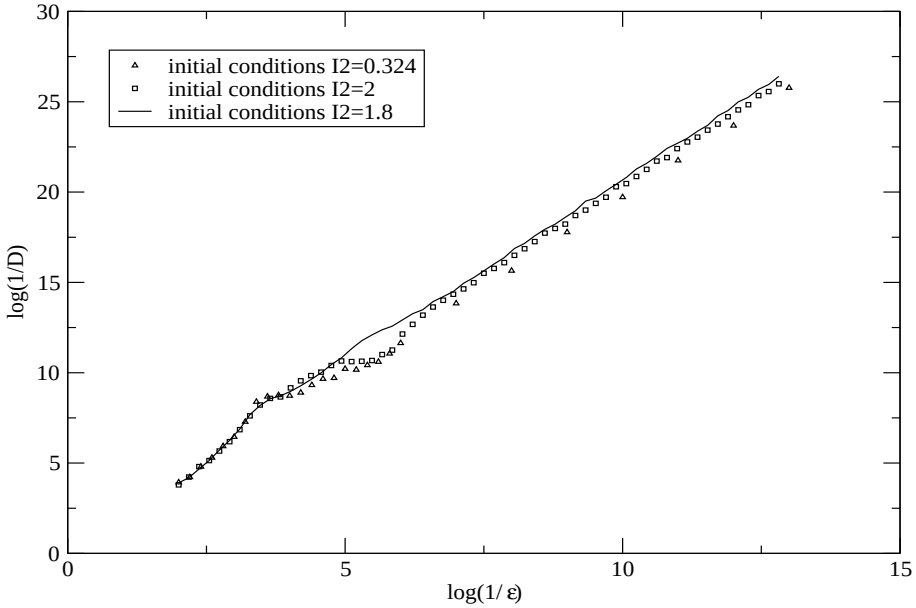

Figure 3: Variation of the diffusion coefficient as a function of ϵ, for $a = 0.4$ and $c = 2.1$. Data are very well fitted to a power law $D(\epsilon) \simeq \epsilon^2$ for $10^{-13} \leq \epsilon \leq 6\,10^{-6}$. For $6\,10^{-6} \leq \epsilon \leq 4\,10^{-4}$ some irregularity can appear depending on the choice of initial conditions, although data are not far from the $D(\epsilon) \simeq \epsilon^2$ law.

of the stable and unstable manifolds of the normally hyperbolic invariant manifold, which, in the continuous case (as the one considered in [6]), is well expressed through explicit integrals. The techniques used in [21], [22] are based on the so–called separatrix map method, which is based on the Melnikov approximation as well.

Here, a Melnikov like approximation, which will be introduced in section 5, is instead based on series expansions which are not explicit. We will compare numerically in section 5 the Melnikov approximations of the stable and unstable manifolds with the representation obtained by the numerical methods described in section 4.

4 Numerical detection of the stable and unstable manifolds

In this section we describe the methods which we use to detect numerically the global structure of the stable and unstable manifolds W_s, W_u of a two dimensional normally hyperbolic invariant manifold of a four dimensional map. We will use two different methods displaying different properties of the global structure of these manifolds. The first one is an extension of the method of propagation of sets commonly used to detect the stable and unstable manifolds of hyperbolic fixed points of two dimensional maps; the second one is based on the computation of the fast Lyapunov indicator (FLI in the following, see [11] and the appendix).

It is well known that the numerical localization of the unstable manifold of an hyperbolic fixed point can be obtained by propagating a small neighborhood of initial conditions up to a time T of the order of some Lyapunov times of the fixed point. In such a way, one directly constructs a neighborhood of a finite piece of the unstable manifold (for the stable manifold one repeats the construction for the inverse flow). This method gives very good results for fixed points of two dimensional maps, because the neighborhoods of the fixed points are two dimensional and can be propagated with reasonable CPU times. A more sophisticated method in the aim of a better visualization of a piece of the manifold can be found in [23].

For higher dimensional maps and higher dimensional invariant hyperbolic manifolds the application of this method encounters two difficulties: the propagation of high dimensional sets requires very long CPU times and the interpretation of the results in an high dimensional space is difficult.

The first problem can be overcome if one knows in advance some approximations of the local unstable manifold to restrict the choice of the set of points to propagate. The second problem could be overcome by reproducing two dimensional sections of the stable and unstable manifolds. However, only few points of the numerically integrated discrete orbits pass near the selected section, so that good results still require enormous sets of initial conditions.

Different sophisticated methods can be found in the literature for computing (un)stable manifolds for higher dimensional cases. The reader can find in [24] a detailed review with applications for the visualization of a 2 dimensional manifold. The common point to all methods is that manifolds are "grown" from local knowledge, i.e. from linear approximations. Then the manifold is constructed as a sequence of geodesic circles. For the specific case of interest here, i.e. for normally hyperbolic invariant manifolds, an algorithm based on graph transform

and Newton's method can be found in [26].

In the following we describe two strategies that allow one to overcome the above problems.

1) Computation and parametrization of $W_s(x)$.

To discuss the properties of the stable and unstable manifolds we need a precise parametrization of these manifolds.

For all values of the parameters a, ϵ the dynamics of $\phi_{|\Lambda}$ is defined by the map (7) which can have invariant KAM curves, resonant librating orbits, resonant chaotic orbits. For the moment we consider $x \in \Lambda$ belonging to a KAM curve of $\phi_{|\Lambda}$, but we will apply the method also to the other cases. As already remarked, the computation of W_u using the method of propagation of sets is simplified by knowing an approximation of $W_u^{loc}(x)$. Here, we use a numerical method valid for $0 < \epsilon < \epsilon_c$ to obtain the linear approximation $x + E^u(x)$ of $W_u^{loc}(x)$.

For a given value of $0 < \epsilon < \epsilon_c$ one has to check if the invariant manifold Λ is still normally hyperbolic. Precisely, we choose the tangent vectors norm: $\|(\xi_{\varphi_1}, \xi_{\varphi_2}, \xi_{I_1}, \xi_{I_2})\|^2 = |\xi_{\varphi_1}|^2 + |\xi_{\varphi_2}|^2 + |\xi_{I_1}|^2 + |\xi_{I_2}|^2$ and we check if the map ϕ^N is hyperbolic for some integer N and for $\epsilon = 0.001$, which is the largest value of the perturbing parameter used in this paper (still lower than ϵ_c). We restrict to a compact invariant region D of Λ, such as the one delimited by two invariant KAM curves. For each point x of a grid of initial conditions with $I_2 \in [0, 2]$, $I_1 = 0$, $\varphi_1 = \pi$, $\varphi_2 = 0$ we first computed the Lyapunov exponents of the map ϕ (up to a $N = 10^3$ iterations) for initial tangent vectors in the tangent space $T_x\Lambda^{ort}$ orthogonal to $T_x\Lambda$, i.e. for vectors of the form $\xi = (\xi_{\varphi_1}, 0, \xi_{I_1}, 0)$. We measured a positive Lyapunov exponent bigger than 0.6 for all the points of the grid, and of course a negative Lyapunov exponent smaller than -0.6 (figure 4 on the left). This is an indication of the hyperbolic splitting of the space $T_x\Lambda^{ort}$ as a direct sum of a stable space $E^s(x)$ and an unstable space $E^u(x)$. The numerical algorithm for the computation of the Lyapunov characteristic exponents provides also an estimate of $\lambda_1 = \mu_1$ and $\lambda_3 = \mu_3$ related to an iterate ϕ^N of ϕ. In fact, if N is sufficiently large, the quantities $1/\exp(FLI(N))$ and $\exp(FLI(N))$, where $FLI(N)$ denotes the Fast Lyapunov indicator computed up to N iterations of the map ϕ, for almost any initial tangent vector $\xi \in T_x\Lambda^{ort}$ converge exponentially to λ_1 and λ_3. It remains to estimate the constants λ_2, μ_2 for the map ϕ^N in the point x. Because in this case the growth of initial tangent vectors $\xi = (0, \xi_{\varphi_2}, 0, \xi_{I_2}) \in T_x\Lambda$ is not expected to be always exponential, we did not computed the Lyapunov characteristic exponents, but we computed numerically the two dimensional matrix representing the restriction of $D\phi^N(x)$ to the space $T_x\Lambda$. This can be done by computing the evolution of a bases of two independent vectors of $T_x\Lambda$. Once the

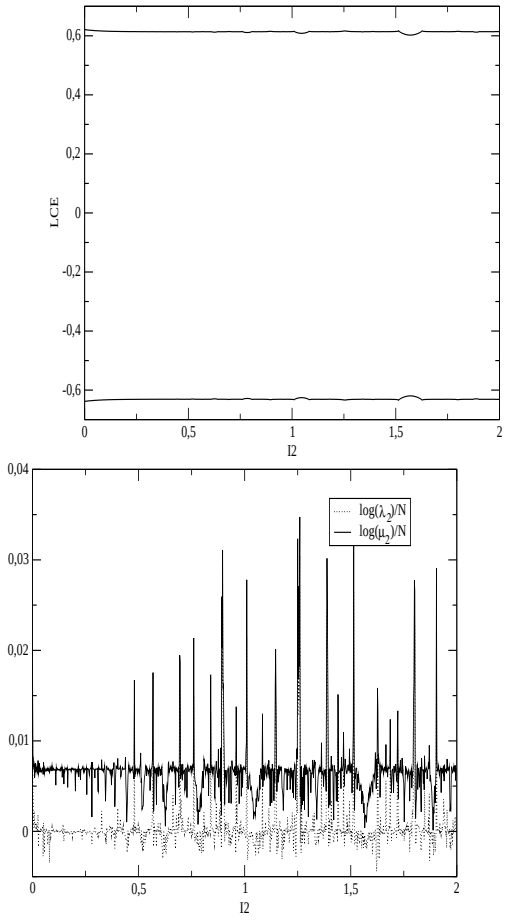

Figure 4: **On the left:** Lyapunov exponents computed on a grid of 1000 initial conditions with $I_2 \in [0, 2]$, $I_1 = 0$, $\varphi_1 = \pi$, $\varphi_2 = 0$, on $N = 10^3$ iterations for $\epsilon = 10^{-3}$. The initial tangent vectors are chosen in the space $T_x\Lambda^{ort}$. A positive and a negative value indicate the splitting of $T_x\Lambda^{ort}$ in a stable and an unstable space. **On the right:** Numerical estimates of $\log \lambda_2/N$ and $\log \mu_2/N$, computed on a grid of 1000 initial conditions with $I_2 \in [0, 2]$, $I_1 = 0$, $\varphi_1 = \pi$, $\varphi_2 = 0$.

matrix $D\phi^N(x)$ was obtained, we computed directly the quantities:

$$\lambda_2 \leq \inf_{\xi \in T_x\Lambda \setminus 0} \frac{\|D\phi^N(x)\xi\|}{\|\xi\|} \leq \sup_{\xi \in T_x\Lambda \setminus 0} \frac{\|D\phi^N(x)\xi\|}{\|\xi\|} \leq \mu_2 \quad .$$

Figure 4 (right panel) shows the numerical computation of $\log \lambda_2/N$ and $\log \mu_2/N$ for $N = 1000$. From the comparison of the four computed quantities $\log \lambda_1$, $\log \lambda_2$, $\log \mu_2$, $\log \lambda_3$ we infer that the invariant manifold Λ is normally hyperbolic.

To compute numerically approximations of the linear space $E^u(x)$ we can now profit of the hyperbolicity of the dynamics. Precisely, we take a generic initial tangent vector $\xi = (\xi_{\varphi_1}, 0, \xi_{I_1}, 0) \in E^s(x) \oplus E^u(x)$ and we define the sequence:

$$\xi_k = D\phi^k(x)\xi = (\xi^k_{\varphi_1}, 0, \xi^k_{I_1}, 0) \in E^s(\phi^k(x)) \oplus E^u(\phi^k(x)) \quad .$$

The evolution of the components $(\xi^k_{I_1}, \xi^k_{\varphi_1})$ does not necessarily reach a limit vector, but we know from hyperbolicity that the component of ξ_k on the space $E^u(\phi^k(x))$ expands exponentially with k, while the component of ξ_k on the space $E^s(\phi^k(x))$ contracts exponentially with k. If the spaces $E^u(\phi^k(x))$, $E^s(\phi^k(x))$ do not converge to fixed directions, as it is expected in the case x lies on an invariant torus, after some iterations of the map the vector ξ_k does not converge to a fixed direction but its direction converges to the unstable direction $E^u(\phi^k(x))$ (the inverse map allows one to obtain $E^s(\phi^k(x))$). Therefore, a strategy to compute the unstable space of a point on an invariant torus is to choose an initial condition x on the torus, and then compute the evolution of a tangent vector for a high (compared to the exponent of the expanding direction) number k of iterations of the map, and then choose as new initial condition the point $\phi^k(x)$ which has the direction $E^u(\phi^k(x))$ determined by ξ_k. For example, in the case of the initial condition $(\varphi_1, \varphi_2, I_1, I_2) = (\pi, 0, 0, 0.324)$, $a = 0.4$, $\epsilon = 10^{-4}$, after $k = 10^5$ iterations we obtain:

$$x \sim (\pi, 4.070625, 0, 0.324319) \quad , \quad E^u(x) \sim < (0.652, 0, 0.75749, 0) >$$

and $x_j = \phi^j(x), E^u(x_j)$ can be easily computed for any needed j.

For any point x_j, denoting by ξ_j the unit vector generating the unstable space $E^u(x_j)$, we use the linear approximation:

$$W^{loc}(x_j) \sim \{x_j + s\ \xi_j \quad , \quad s \in [0, \rho)\} \quad ,$$

which is good as soon ρ is very small (we use $\rho = 10^{-10}$ in our computations).

Then, from the knowledge of the linear approximation of the local manifold we compute finite pieces of the unstable manifold using:

$$\phi^j(W^{loc}_u(x_{-j})) \subseteq W_u(x) \quad .$$

The small error that we do in using the linear approximation for the local manifold do not accumulate at successive iterations, because the hyperbolic dynamics tends to reduce these errors at successive iterations. Being interested also in computing a parametrization of the manifold with respect to its arc length, we proceed in two steps. First, we set K such that:

$$W_1(x) = \cup_{j=1}^{K} \phi^j(W_u^{loc}(x_{-j})) \subseteq W_u(x)$$

can be parametrized by the φ_1 coordinate, so that we can order the points in $W_1(x)$ with respect to φ_1 (figure 5, left). This allows one to construct a parametrization of $W_1(x)$ with respect to its arc–length, that we denote:

$$s \longmapsto (\varphi_1(s), \varphi_2(s), I_1(s), I_2(s)) \quad .$$

Then, we want to reconstruct the unstable manifold also for an arc–length much longer than the one obtained at the first step, so that to include many lobes of the manifold. This can be easily done by mapping with ϕ^K additional points of the linear approximation of the local manifold (figure 5, right panel), but paying attention to obtain a uniform sampling of the manifold with respect to its arc–length. This problem was already discussed in [23] and we use a similar procedure for the choice of the initial conditions on $W_u^{loc}(x_{-K})$. More precisely, let us denote by x^m, x^{m+1} the last two points of $W_u^{loc}(x_{-K})$ used to compute $W_1(x)$, by $\Delta x^m = d(x^m, x^{m+1})$, and by $\Delta s^m = s^{m+1} - s^m$ the difference of the arc–lengths of the points $\phi^K(x^m)$,$\phi^K(x^{m+1})$. The choice of the point x^{m+2} will be done depending on Δs^m as follows:

$$\begin{cases} x^{m+2} = x^{m+1} + \Delta x^m & \text{if} \quad \Delta s_1 < \Delta s^m < \Delta s \\ x^{m+2} = x^{m+1} + \eta \Delta x^m & \text{if} \quad \Delta s^m > \Delta s \\ x^{m+2} = x^{m+1} + \frac{1}{\eta} \Delta x^m & \text{if} \quad \Delta s^m < \Delta s_1 \end{cases} \tag{8}$$

with $\Delta s, \Delta s_1, \eta$ suitable parameters, which we set to $\Delta s = 10^{-2}$, $\Delta s_1 = 10^{-3}$ and $\eta = 0.1$ in our numerical experiments.

2) Detection of stable manifolds using the Fast Lyapunov Indicator

We have found a new application of the FLI method which allows one to obtain a sharp detection of the intersection of the stable and unstable manifolds of the normally hyperbolic invariant manifolds with any two dimensional surface of the phase–space. The principle is the following. We sample the two dimensional surface of the phase space with a grid of points. Then, for any point of the grid we compute the FLI (see Appendix) up to a time T. The points of the grid which

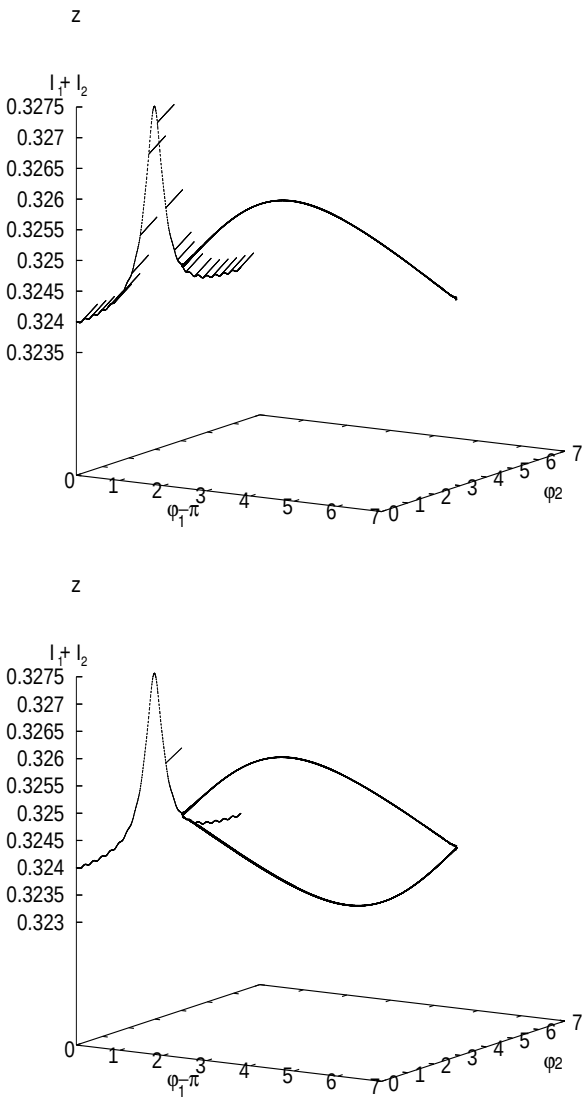

Figure 5: Sketch of the first (left panel) and second (right panel) step of the algorithm of computation of the unstable manifold. The coordinates of the plot are: $(\varphi_1-\pi, \varphi_2, I_1+I_2)$. One invariant torus of the map restricted to Λ is plotted. We recall that $\varphi_1 = \pi$ and $I_1 = 0$ on Λ. (Left panel) The segments correspond to the local linear approximation of the unstable manifold of the points x_{-j}, $j = 1, ...K$. The flow ϕ^j applied on such points allows one to construct $W_1(x)$ (the "arc-shaped" structure), with x selected in Λ as explained in the text. (Right panel) Some of the points x_{-K} are plotted (the segment in the picture). The flow ϕ^K allows one to add ordered points to the manifold $W_u(x)$. In order to have a uniform sampling of the manifold with respect to its arc length the choice of the points x_{-K} is adapted to the evolution of the arc parameter of the manifold as explained in the text.

will have the highest values of the FLI are those points whose orbits approach an hyperbolic invariant manifold within the time T, because the growth of tangent vectors is bigger near the hyperbolic manifolds. Therefore, a short–time computation of the FLI allows one to detect a neighborhood of a finite piece of the stable manifold (for the unstable manifold one repeats the computation using the inverse map). As a check on a well known example, we show in figure 6 the computation of the FLI on a set of 900×900 initial conditions regularly spaced in I, φ for the standard map of equations:

$$\varphi' = \varphi + I \quad , \quad I' = I + a \sin \varphi' \tag{9}$$

with $a = 0.3$, iterated up to $T = 100$. In such a case KAM tori have $FLI \sim \log(T)$, while higher values characterize chaotic orbits and lower values characterize regular resonant motion [12],[13],[14]. In figure 6 for any initial condition with $\varphi \in [-0.1, 0.1]$, $I \in [-0.1 : 0.1]$ we plot the value of the FLI after T iterations of the map ($T = 100$ on the left panel and $T = 1000$ on the right panel) using a color scale[1] such that the orange and yellow structures correspond to pieces of the stable manifold. For comparison, the black points on the chaotic region of figure 6, left represent the stable manifold obtained with the classical method of propagation of sets (see the figure caption). The agreement among the results of the two methods is good and in particular we remark the sensitivity of the FLI method.

When increasing the number of iterations (right panel of figure 6) the whole chaotic zone surrounding the origin appears clearly, but the manifold structure is lost as well as when increasing the integration time in the method of propagation of a set of initial conditions.

The advantage of the FLI method is that it is not sensitive to the dimension of the phase–space, and that one does not need to know in advance which are the normally hyperbolic invariant manifolds and their local approximations. In fact, the method detects the stable manifolds of all the hyperbolic structures of the system.

5 Topology of the stable and unstable manifolds

In this section we compute different representations of the stable and unstable manifolds of Λ for $a > 0$. When $\epsilon = 0$ the stable and unstable manifolds W_s, W_u of Λ are the product of the stable and unstable

[1]The color version of all figures can be found on the electronic version of the paper so that light gray corresponds there to yellow and darker grey corresponds there to darker orange.

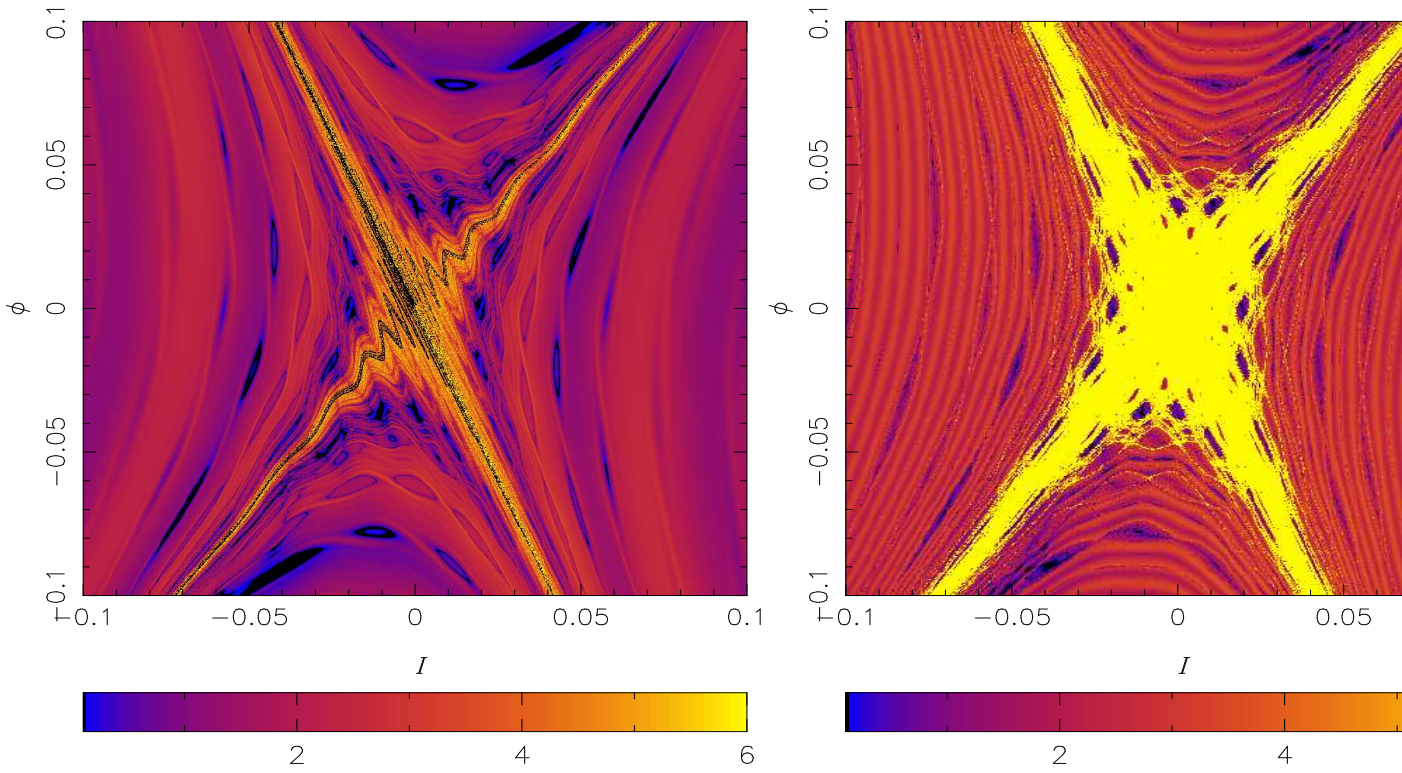

Figure 6: Representation of the FLI for the standard map (9). For any initial condition with $\varphi \in [-0.1, 0.1]$, $I \in [-0.1, 0.1]$ we plot the value of the FLI after $T = 100$ (left panel) and $T = 1000$ (right panel) iterations of the map using a color scale. **On the left:** with the short number of $T = 100$ iterations we detect a finite piece of the stable manifold. The black points on the chaotic region represent the stable manifold obtained with the classical method of propagation of a set of 1000 initial conditions in a neighborhood of size 10^{-10} of the hyperbolic fixed point $(0, 0)$, up to 100 iterations. **On the right:** For the longer integration time $T = 1000$ the whole chaotic zone surrounding the origin appears clearly, but the manifold structure is lost as well as when increasing the integration time in the method of propagation of a set of initial conditions.

manifolds W_s^*, W_u^* of the hyperbolic fixed point of the standard map:

$$\varphi_1' = \varphi_1 + I_1 \quad , \quad I_1' = I_1 - a \sin \varphi_1' \tag{10}$$

with the torus $\mathbb{T}^2$, domain of (φ_2, I_2); W_s intersects W_u at any intersection point of W_s^*, W_u^*; there is no diffusion in the variable I_2.

To study diffusion along Λ it is convenient to consider the two dimensional surface of the phase–space:

$$S = \{(\varphi_1, \varphi_2, I_1, I_2) \text{ such that } : \varphi_1 = \pi \quad , \quad \varphi_2 = 0\} \tag{11}$$

which we already used in figure 2 to represent the spread of orbits with initial condition in a neighborhood of S. In the following we describe and compute the topology of the sets:

$$S_u^* = \cup_{x \in \Lambda} \Big(S \cap W_u(x) \Big) \quad , \quad S_s^* = \cup_{x \in \Lambda} \Big(S \cap W_s(x) \Big) \quad .$$

Any invariant torus of $\phi_{|\Lambda}$ intersects S_u^* in only one point x, so that S_u^* is the set where points with initial conditions in a neighborhood of S can return near S following diffusion paths defined by the unstable manifolds of the points of Λ. When $\epsilon = 0$ it is:

$$S_u^* = \{(\varphi_1, \varphi_2, I_1, I_2) \text{ such that } : \varphi_1 = \pi \ , \ (I_1, \varphi_1) \in W_u^* \ , \ \varphi_2 = 0\} \ ,$$

that is a set of lines parallel to the I_2 axis with accumulations. The same holds for S_s^*. When $\epsilon \neq 0$ understanding the topology of S_u^*, S_s^* becomes a difficult problem, but if ϵ is very small, we can use Melnikov like approximations.

A Melnikov–like approximation of S_u^*

The Melnikov approximations of a priori unstable systems are obtained by neglecting the perturbation on the hyperbolic part of the system, which is usually chosen to be integrable by quadratures. Here, the unperturbed hyperbolic part of the system is represented by the standard map (10), which is not integrable. Nevertheless, we define a Melnikov–like approximation:

Definition. *Let us consider $x = (\varphi_1, \varphi_2, I_1, I_2) \in \Lambda$ and denote $J = I_2$. We define the Melnikov approximation of $W_u(x)$ to be the unstable manifold of x with respect to the following simplified map $\tilde{\phi}$:*

$$\begin{aligned} \varphi_1' &= \varphi_1 + I_1 \qquad & \varphi_2' &= \varphi_2 + J \\ I_1' &= I_1 - a \sin \varphi_1' \qquad & I_2' &= I_2 + \epsilon \frac{\sin \varphi_2'}{(\cos \varphi_1' + \cos \varphi_2' + c)^2} \end{aligned} \quad . \tag{12}$$

We can represent the Melnikov approximation of $W_u(x)$ as follows:

Proposition. *Let us consider* $x = (\tilde{\varphi}_1, \tilde{\varphi}_2, \tilde{I}_1, \tilde{I}_2) \in \Lambda$ *and denote* $J = \tilde{I}_2$. *The Melnikov approximation of* $W_u(x)$ *can be obtained by all points* $z = (\varphi_1, \varphi_2, I_1, I_2)$ *such that* (φ_1, I_1) *is in the unstable manifold* W_u^* *of the fixed point* $(\pi, 0)$ *with respect to the map:*

$$\varphi_1' = \varphi_1 + I_1 \quad , \quad I_1' = I_1 - a \sin \varphi_1' \quad , \tag{13}$$

while $\varphi_2 = \tilde{\varphi}_2$ *and:*

$$I_2 = \tilde{I}_2 - \epsilon \sum_{k=-1}^{-\infty} \Big(\frac{\sin(\tilde{\varphi}_2 - kJ)}{(\cos\varphi_1(k) + \cos(\tilde{\varphi}_2 - kJ) + c)^2} - \frac{\sin(\tilde{\varphi}_2 - kJ)}{(\cos(\tilde{\varphi}_2 - kJ) + c - 1)^2} \Big) \tag{14}$$

where $(\varphi_1(j), I_1(j))$ *denote the orbit with initial condition* $(\varphi_1, I_1) \in W_u^*$ *with respect to the map (13).*

The proof of this proposition is reported at the end of this section. Here, we use the proposition to obtain a parametric representation of the unstable manifold W_u in the Melnikov approximation. In figure 7 we report the plot of two parametrizations $s \mapsto (I_2(s) - I_2(0))$: one is obtained with the Melnikov approximation (14), while the other one is obtained using the full map and the method described in section 4. The left panel shows that for $\epsilon = 10^{-6}$ the two parametrizations are indeed very close one to the other. The right panel shows that for $\epsilon = 10^{-4}$ the Melnikov approximation is no valid at all.

In order to appreciate the accuracy of the Melnikov approximation we have computed for $10^{-8} < \epsilon < 10^{-3}$ the histogram of $(I_2(s) - I_2(0))/\epsilon$ for both the full map and the Melnikov approximation. We consider as an indicator of the distance between the two distributions the quantity:

$$d = \frac{\sum_{i=1}^{N} (H_f(i) - H_M(i))^2}{N} \tag{15}$$

where H_f and H_M correspond to the histograms of $(I_2(s) - I_2(0))/\epsilon$ for respectively the full map and the Melnikov approximation and $N = 100$ is the number of bins. The quantity d (figure 8) remains smaller than $3\,10^{-6}$ up to $\epsilon = 5\,10^{-6}$ and suddenly increases with ϵ, although not regularly, for higher values of the perturbing parameter. We remark that the transition value $5\,10^{-6}$ is close to the transition value from a regular to an irregular behavior of the diffusion coefficient (figure 3).

In order to describe the topology of S_u^* using the Melnikov approximation, we define the sequence s_k, $k \in \mathbb{N}$, such that $\varphi_1(s_k) = \pi$, so that the Melnikov approximation of S_u^* is:

$$S_u^* = \cup_{k \in \mathbb{N}} (\varphi_1(s_k), 0, I_1(s_k), I_2(s_k)) \quad ,$$

that is a set of lines parallel to the I_2 axis with accumulations, as in the unperturbed case. As a consequence, when the topology of finite

pieces of S^* is very far from lines parallel to the I_2 axis, the system is very far from the validity of the Melnikov approximation regime. We describe below the detection of a transition in the topology of the sets S_u^*, S_s^* which turns out to correspond to the loose of validity of the Melnikov approximation.

A transition in the topology of S_s^*, S_u^*

We considered the map (5) with $c = 2.1$, $a = 0.4$ and we computed S_s^* for different values of ϵ by computing the FLI on refined grids of 1000×1000 regularly spaced points of S. The results are shown in figures 9,10[2]: the three columns of the figures represent different zooms of S with respect to the action I_1, allowing one to appreciate the topology of S_s^* from the small values of $I_1 \in [10^{-11}, 10^{-8}]$ (left column) up to I_1 of order 0.1 (right column). Each line refers to a different value of ϵ, so that we can appreciate the evolution of S_s^* from $\epsilon = 0$ up to ϵ of order 10^{-3}. The action I_2 is in the range $[0, 1]$. We now comment the results. For $\epsilon = 0$ (top line of figure 9) we recognize that S_s^* is a set of lines parallel to the axis $I_1 = 0$ with accumulation towards $I_1 = 0$, as we expected. For $\epsilon = 10^{-6}$ (second line of figure 9) the situation is very similar to the case with $\epsilon = 0$: S_s^* seems to be represented by vertical lines (of course with small deviations), as it is expected if the Melnikov approximation is valid. For $\epsilon = 6\ 10^{-6}$ (last line of figure 9) most of the vertical lines are still visible in the three zooms, though with an evident distortion. However, the vertical lines have disappeared in some regions. For $\epsilon = 4\ 10^{-5}$ (top line of figure 10) we are close to a transition in the topology of all vertical lines, which becomes more evident for $\epsilon = 6\ 10^{-5}$ (second line of figure 10), where horizontal lines appear. This kind of topology cannot be explained by the Melnikov approximation, which is therefore not valid for this value of ϵ. For $\epsilon = 6\ 10^{-4}$ (last line of figure 10) the transition in the topology of S_s^* is complete: the inner zoom shows only horizontal lines and also the outer zoom reveals a topology which is completely different from the one which is expected in the Melnikov approximation. We say that for this value of ϵ the transition of the topology of S_s^* in the range of $I_2 \in [0, 1]$ is completed.

We repeated these computations for $I_2 \in [1.4, 2.4]$, and we detected the same kind of transitions in the topology of S_s^*.

Summarizing these results, we have shown that for small values of ϵ the topology of S_s^* is consistent with the description of the stable (unstable) manifolds obtained with the Melnikov approximation, i.e.

[2]To better appreciate the topology we uploaded high resolution pictures available also at *http://www.obs-nice.fr/elena/topology*. In the final version of the paper the pictures should be available on-line as supplemental material.

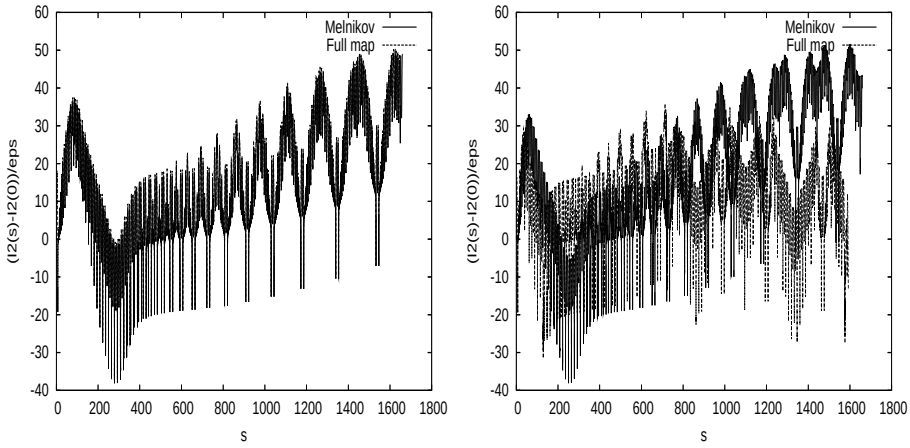

Figure 7: Each panel represents two parametrizations $s \mapsto (I_2(s) - I_2(0))/\epsilon$: one is obtained with Melnikov approximation, while the other one is obtained using the full map. The left panel is for $\epsilon = 10^{-6}$: the two parametrizations are close one to the other. The right panel is for $\epsilon = 10^{-4}$: the Melnikov approximation is not valid.

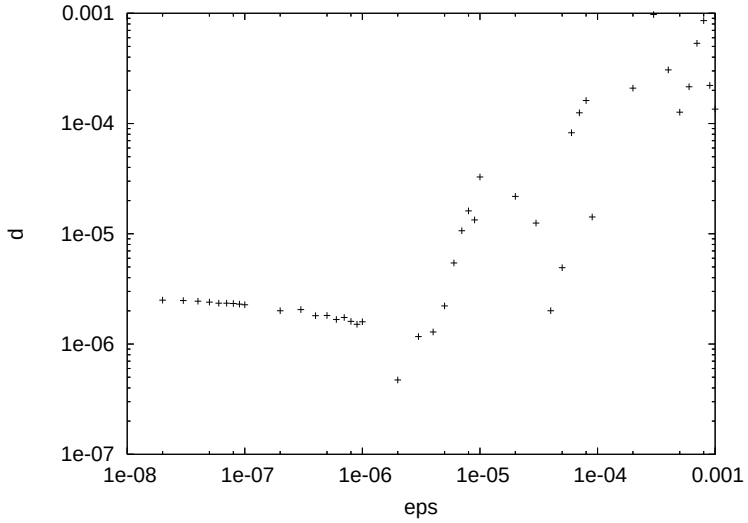

Figure 8: Computation of d defined in (15) as a function of ϵ. We can appreciate that d remains smaller than $3\,10^{-6}$ up to $\epsilon = 5\,10^{-6}$. For higher values of the perturbing parameter d suddenly increases with ϵ, although not regularly.

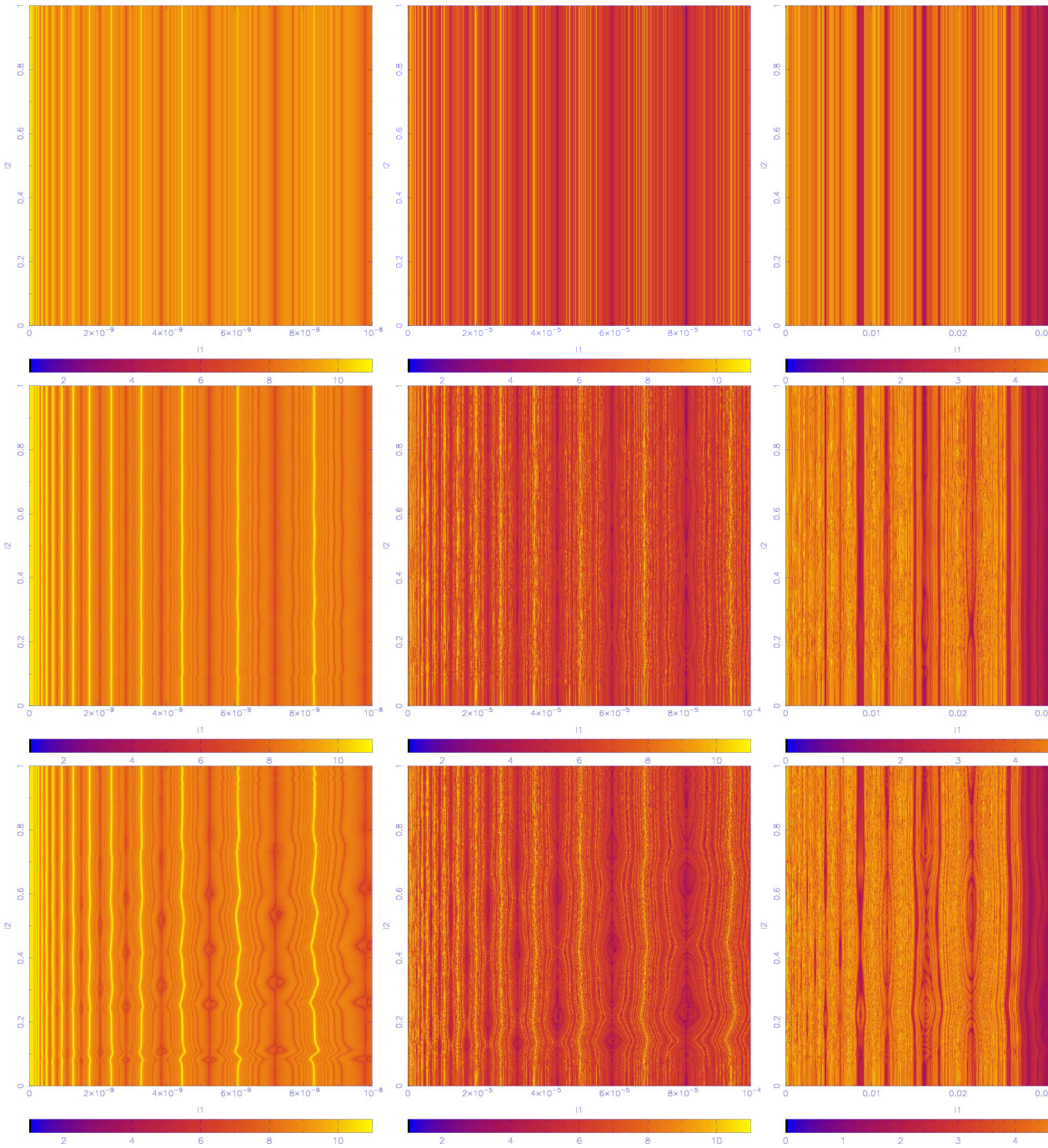

Figure 9: Computation of S_s^* for $I_1 < 10^{-8}$ ($t = 60$, left panels), for $I_1 < 10^{-4}$ ($t = 80$, middle panels) and $I_1 < 10^{-2}$ ($t = 80$, right panels). The perturbation is (from top to bottom) $\epsilon = 0, 10^{-6}, 6\ 10^{-6}$. The yellow lines correspond to finite pieces of the stable manifold.

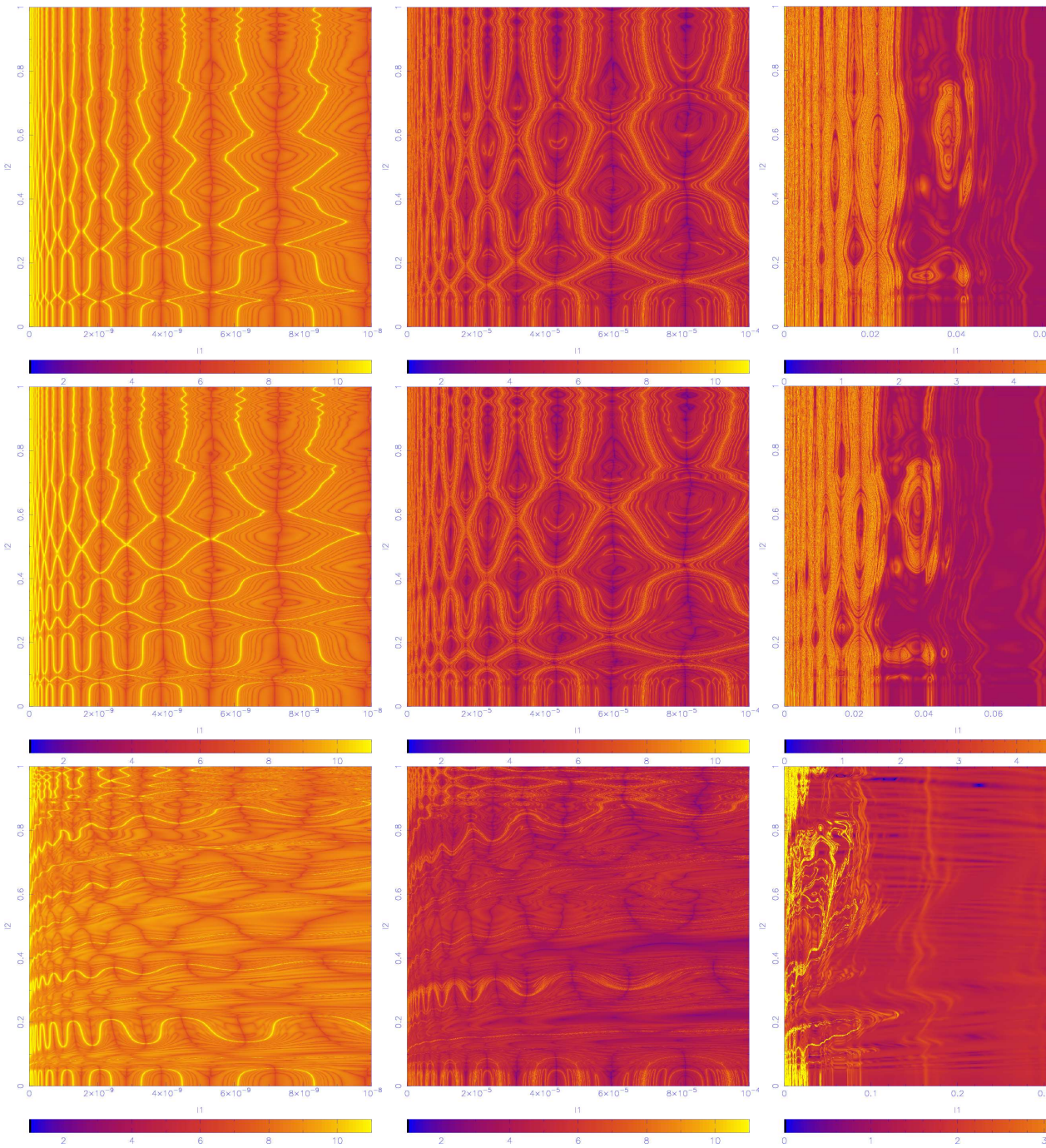

Figure 10: Computation of S_s^* for $I_1 < 10^{-8}$ ($t = 60$, left panels), for $I_1 < 10^{-4}$ ($t = 80$, middle panels) and $I_1 < 10^{-2}$ ($t = 80$, right panels). The perturbation is (from top to bottom) $\epsilon = 4\ 10^{-5}, 6\ 10^{-5}, 6\ 10^{-4}$. The yellow lines correspond to finite pieces of the stable manifold.

it is characterized by the prevalence of vertical lines. For high values of ϵ the topology is characterized by horizontal lines which originate at the resonances on Λ. This happens even for values of ϵ such that the restricted map has still al lot of invariant tori, so that the transition in the topology of S_s^* is not related to the transition to the Chirikov regime of $\phi_{|\Lambda}$. For intermediate values of ϵ we detect a transition among the two topologies, in which the vertical lines are distorted up to be completely replaced by horizontal lines.

We find useful to compare the different topologies of S_s^* with the dependence of the diffusion coefficient on ϵ that we represented in figure 3, where we identified a law for the diffusion coefficient $D \sim \epsilon^2$ for $\epsilon < \epsilon_1 \sim 6\ 10^{-6}$ approximately some irregular behavior up to $\epsilon = \epsilon_2$, which is about $4\ 10^{-4}$, and then a different regular power law for $\epsilon > \epsilon_2$. We remark that the interval (ϵ_1, ϵ_2) corresponds approximately to the interval of transition from the topology characteristic of the Melnikov approximation to the completely different topology characterized by the horizontal structures, so that the topology of the stable (unstable) manifold and the dependence of the diffusion coefficient on ϵ are correlated.

Proof of the Proposition

Let us denote by $z(j) = (\varphi_1(j), \varphi_2(j), I_1(j), I_2(j))$ the orbit of $z = z(0) = (\varphi_1, \varphi_2, I_1, I_2)$ and by $x(j) = (\tilde{\varphi}_1(j), \tilde{\varphi}_2(j), \tilde{I}_1(j), \tilde{I}_2(j))$ the orbit of $x = \tilde{x}(0) = (\tilde{\varphi}_1, \tilde{\varphi}_2, \tilde{I}_1, \tilde{I}_2)$ with respect to the map ϕ. The point z is in the unstable manifold of x if and only if it is:

$$\lim_{j \to -\infty} \|z(j) - x(j)\| = 0 \quad .$$

Therefore, $(I_1(j), \varphi_1(j))$ tends to $(0, \pi)$ as $j \to -\infty$ if and only if $(I_1(0), \varphi_1(0))$ is in the unstable manifold W^u of the fixed point $(\pi, 0)$ with respect to the map (13). Let us now prove (14). For any $j \leq -1$ it holds:

$$I_2(j) = \sum_{k=-1}^{j} (I_2(k) - I_2(k+1)) + I_2(0) = \epsilon \sum_{k=-1}^{j} \frac{\sin \varphi_2(k+1)}{(\cos \varphi_1(k+1) + \cos \varphi_2(k+1) + c)^2} + I_2 \quad ,$$

as well as:

$$\tilde{I}_2(j) = \sum_{k=-1}^{j} (\tilde{I}_2(k) - \tilde{I}_2(k+1)) + \tilde{I}_2(0) = \epsilon \sum_{k=-1}^{j} \frac{\sin \tilde{\varphi}_2(k+1)}{(\cos \tilde{\varphi}_2(k+1) + c - 1)^2} + \tilde{I}_2 \quad .$$

Therefore, it is:

$$\lim_{j \to -\infty} \|I_2(j) - \tilde{I}_2(j)\| = 0$$

if and only if it holds (14).

6 Spread of the unstable manifolds and diffusion

We computed the parametrization of $W_u(x)$ using the first method reported in section 4 for quite a long arc–length for different values of $0 < \epsilon < \epsilon_c$ ($a = 0.4$, $c = 2.1$) and for different types of orbits of $\phi_{|\Lambda}$, KAM tori, regular resonant librations and resonant chaotic motions.

In figures 11, 12, 13 (top right panels) it appears clearly that $I_2(s)$ undergoes large fluctuations for all the kind of different dynamics. The unstable manifolds, which are contained in a plane $I_2 = constant$ for $\epsilon = 0$, are unrolled along the I_2 direction for $\epsilon > 0$, thus supporting diffusion in the neighborhood of Λ. To appreciate that the manifolds are unrolled in the phase–space we represent them (bottom right panels) in the three–dimensional space φ_1, I_1, I_2. The reference orbits of the restricted map are instead represented in the bottom left panels. To measure the spread of the manifolds in the I_2 direction we also plot on the bottom left panels the vertical segments which correspond to the representation on the plane (I_2, φ_2) of the points of $W_u(x)$ with $|\varphi_1 - \pi| \leq 0.5$ (reducing the tolerance on φ_1 decreases the number of points on the figure, but does not decrease the amplitude of the segment). For the case of the KAM torus (figure 11) for $\epsilon = 10^{-6}$ this segment is definitely bigger than the variation of I_2 along the torus. For the case of the resonant regular libration and the chaotic orbit for $\epsilon = 10^{-4}$ (figures 12, 13) the amplitudes of respectively 2 10^{-3}, 1.5 10^{-3} of these segments are representative of the spread of $W_u(x)$ along the I_2 direction.

We remark that these conclusions are obtained for a value of ϵ for which the Melnikov approximation is valid ($\epsilon = 10^{-6}$) as well as for a value for which the Melnikov approximation is not accurate, but the dynamics of $\phi_{|\Lambda}$ is still bounded by many invariant tori.

From figures 11, 12, 13, we observed that the unstable manifolds are characterized by many oscillations in the I_2 direction which remember us the oscillation that the actions do in diffusing along the resonances. Therefore, to remove the effect of the oscillations and to look for a systematic spread of the manifolds in the I_2 direction we compute the quadratic averages of the quantity $I_2(s) - I_2(0)$ with respect to many close initial points x. Precisely, in figure 14 we represented:

$$d(s) = \frac{1}{N} \sum_{j=1}^{N} \left(I_2^j(s) - I_2^j(0) \right)^2 \tag{16}$$

versus s for $\epsilon = 10^{-5}$ ($N = 200$, the initial conditions are $I_1 = 0$, $\varphi_1 = \pi$, $0.6 < I_2 < 1$, $\varphi_2 = 0$). The figures remark a systematic growth of the quadratic spread of the manifolds. The large oscillations

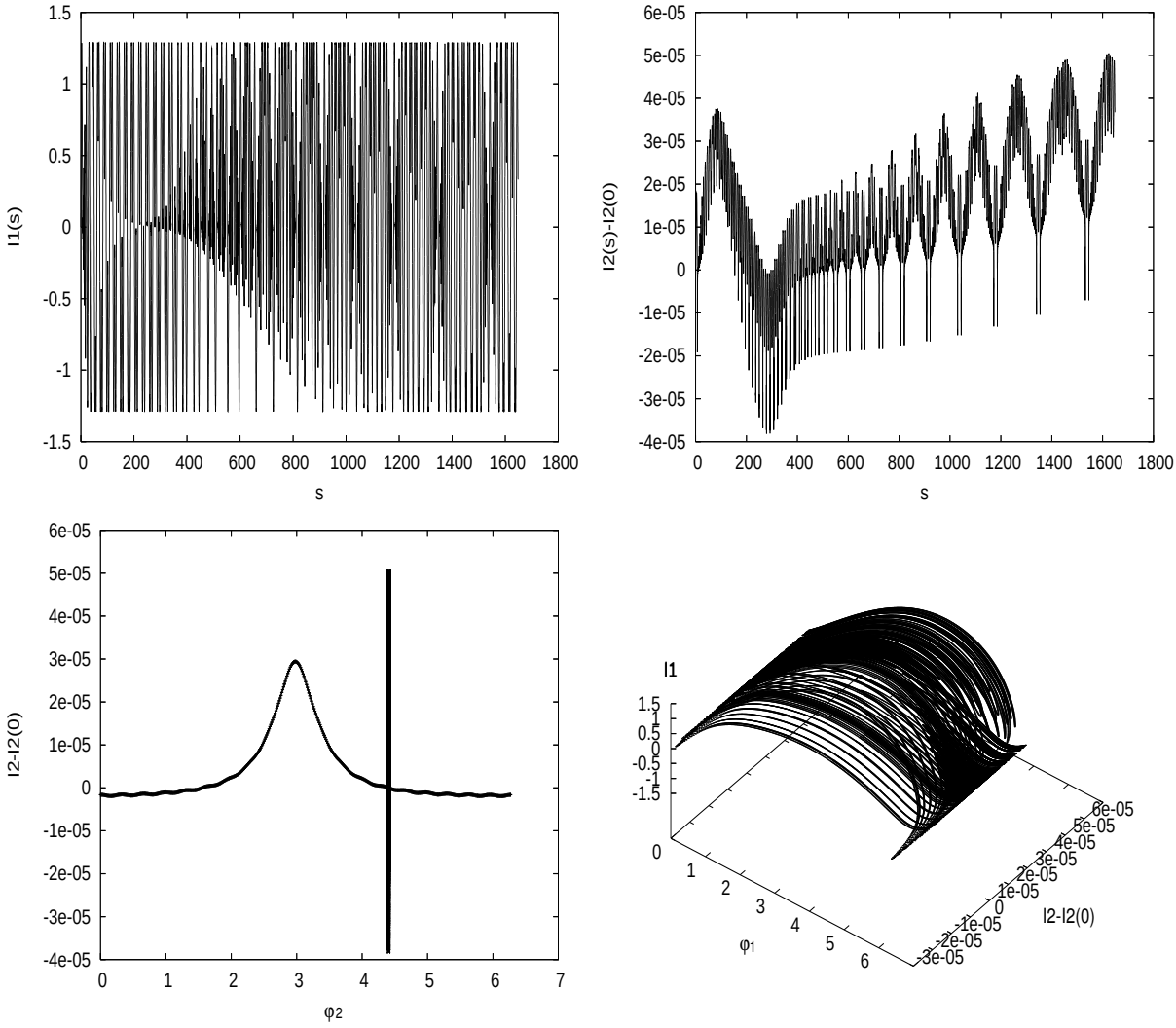

Figure 11: Computation of the unstable manifold for an initial condition $(\varphi_1, \varphi_2, I_1, I_2) = (\pi, 0, 0, 0.324)$ on a KAM torus of $\phi_{|\Lambda}$ for $\epsilon = 10^{-6}$. The initial conditions for the computation of the manifold after $k = 10^5$ iterations are $x = (\pi, 4.406484, 0, 0.324001)$. **On the top:** Representation of $I_1(s)$ (on the left) and $I_2(s)$ (on the right). **On the bottom left:** The orbit of $\phi_{|\Lambda}$ is on a KAM torus. The vertical segment corresponds to the representation on the plane $(I_2 - I_2(0), \varphi_2)$ of the points of $W_u(x)$ with $|\varphi_1 - \pi| \leq 0.5$ (reducing the tolerance on φ_1 decreases the number of points on the figure, but does not decrease the amplitude of the segment). The fluctuations of $W_u(x)$ along I_2 are definitely bigger than the variation of I_2 along the torus. **On the bottom right:** Representation of the unstable manifold of x in the three dimensional space φ_1, $I_2 - I_2(0)$,I_1.

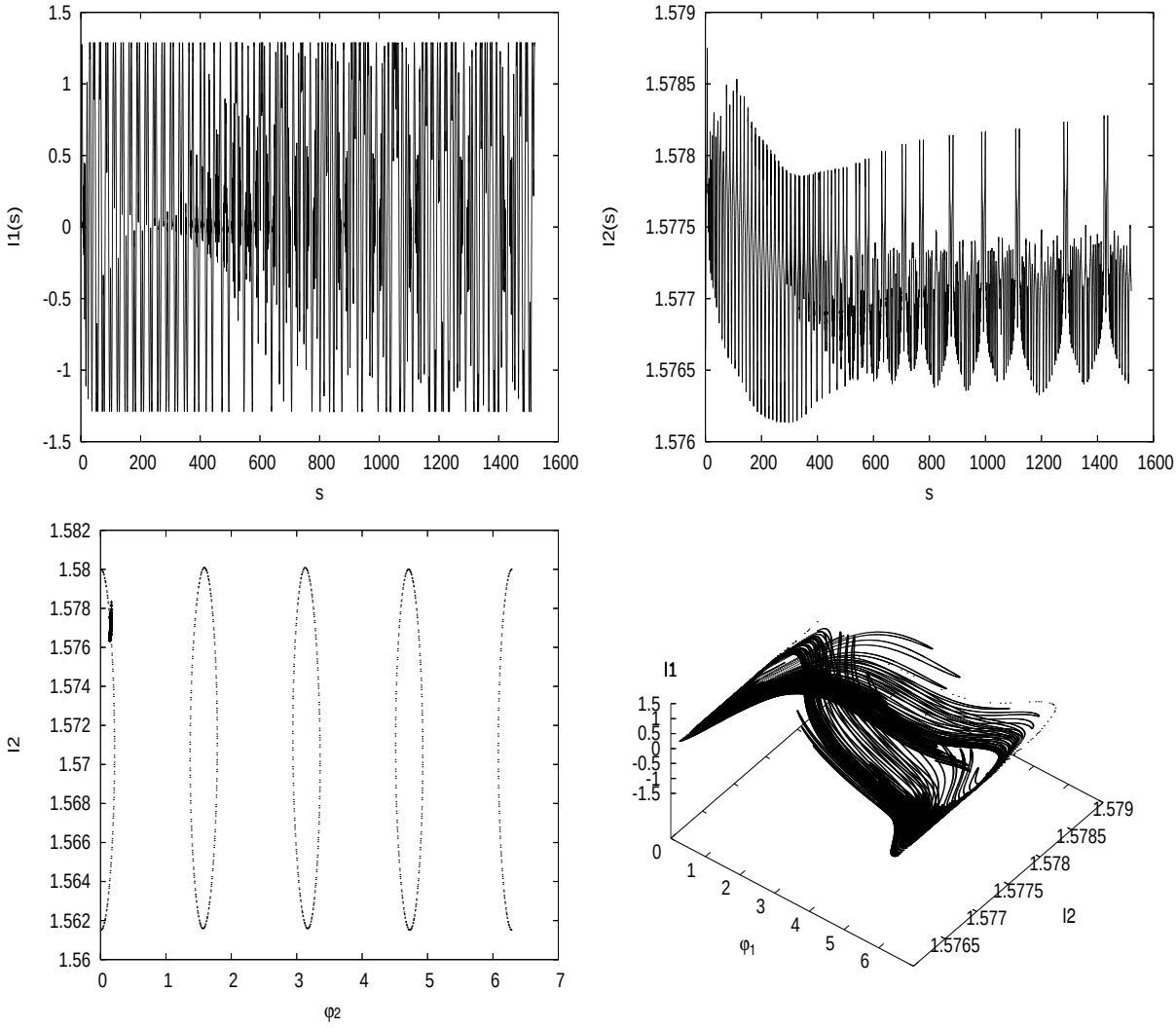

Figure 12: Computation of the unstable manifold for an initial condition $(\varphi_1, \varphi_2, I_1, I_2) = (\pi, 0, 0, 1.58)$ on a regular resonant libration of $\phi_{|\Lambda}$ for $\epsilon = 10^{-4}$. The initial conditions for the computation of the manifold after $k = 10^5$ iterations are $x = (\pi, 0.153, 0, 1.576)$. **On the top:** Representation of $I_1(s)$ (on the left) and $I_2(s)$ (on the right). **On the bottom left:** The orbit of $\phi_{|\Lambda}$ is on a regular resonant libration. The small vertical segment corresponds to the representation on the plane (I_2, φ_2) of the points of $W_u(x)$ with $|\varphi_1 - \pi| \leq 0.5$ (reducing the tolerance on φ_1 decreases the number of points on the figure, but does not decrease the amplitude of the segment). The amplitude of 2 10^{-3} of this segment in the direction of I_2 is representative of the spread of $W_u(x)$ along this direction. **On the bottom right:** Representation of unstable manifold of x in the three dimensional space φ_1, I_2,I_1.

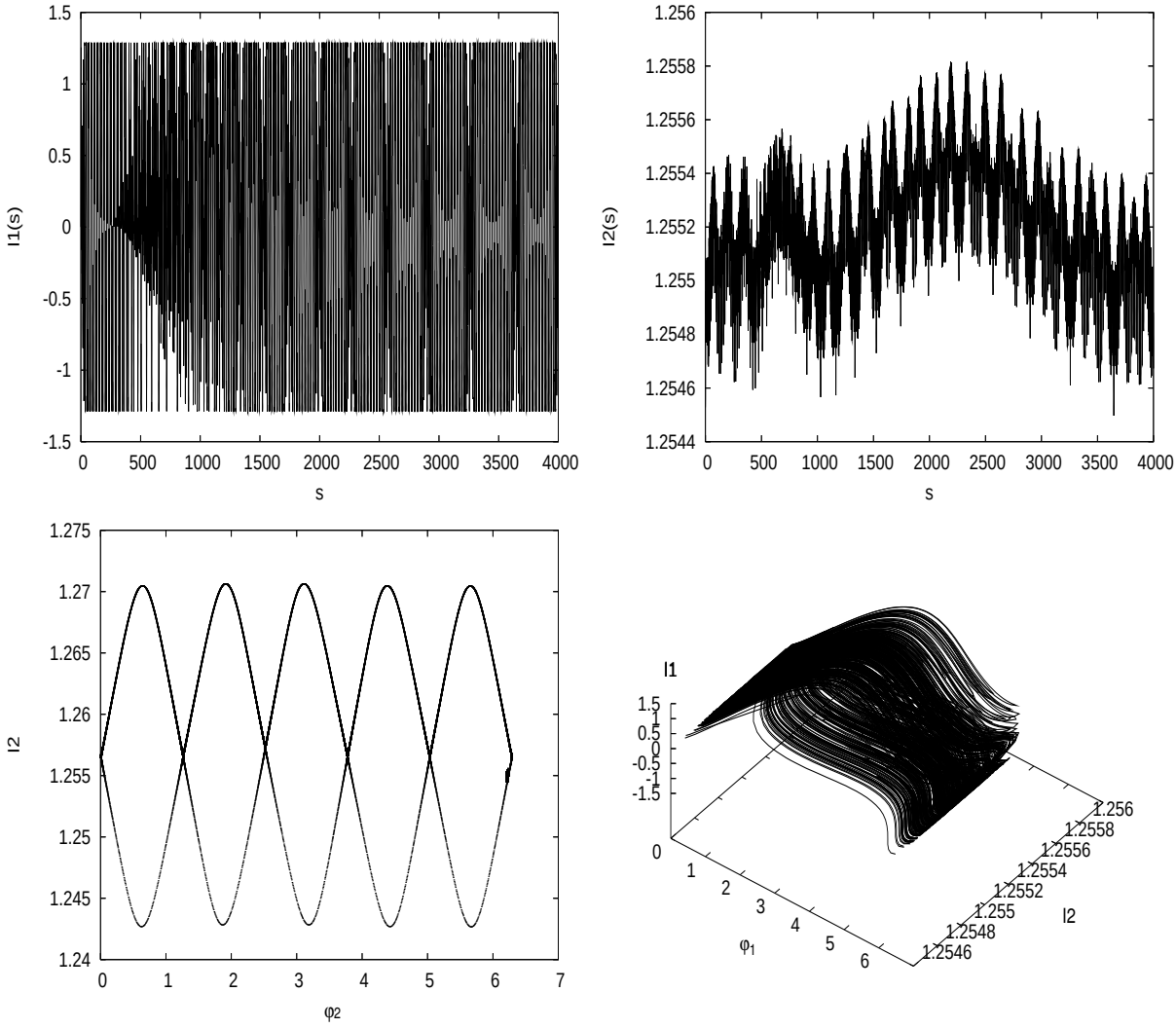

Figure 13: Computation of the unstable manifold for an initial condition $(\varphi_1, \varphi_2, I_1, I_2) = (\pi, 0, 0, 1.256)$ on a chaotic resonant orbit of $\phi_{|\Lambda}$ for $\epsilon = 10^{-4}$. The initial conditions for the computation of the manifold after $k = 10^5$ iterations are $x = (\pi, 6.213, 0, 1.254)$. **On the top:** Representation of $I_1(s)$ (on the left) and $I_2(s)$ (on the right). **On the bottom left:** The orbit of $\phi_{|\Lambda}$ is chaotic. The small vertical segment corresponds to the representation on the plane (I_2, φ_2) of the points of $W_u(x)$ with $|\varphi_1 - \pi| \leq 0.5$ (reducing the tolerance on φ_1 decreases the number of points on the figure, but does not decrease the amplitude of the segment). The amplitude of $1.5\ 10^{-3}$ of this segment in the direction of I_2 is representative of the spread of $W_u(x)$ along this direction. **On the bottom right:** Representation of unstable manifold of x in the three dimensional space φ_1, I_2,I_1.

are due to the excursions of I_2 with respect to φ_1. We can kill them both computing a running average on eq. (16), or taking the values of $I_2(s)$ with $\varphi_1(s)$ on a suited small interval as shown in figure 14, left panel. Finally, to provide a quantitative measure of the link between diffusion of orbits and geometric spread of the unstable manifolds we define a "geometrical" diffusion coefficient of the unstable manifolds. At this purpose, if we consider the restriction of the map ϕ to the unstable manifold, the arc–length s grows nearly exponentially with time when the manifold passes near the hyperbolic invariant manifold. By denoting with λ the mean value of the Lyapunov exponent computed over a time of $t = 10^9$ iterations (for a set of $N = 20$ orbits with initial conditions: $-10^{-5} < I_1 < 10^{-5}$, $\varphi_1 = \pi$, $0.3 < I_2 < 3$, $\varphi_2 = 0$), we define the "geometrical" diffusion coefficient μ as the limit slope of the quantity:

$$G(t) = \frac{\lambda d(s(t))}{\ln(s(t)/s(0))} \quad , \tag{17}$$

where we defined $s(t) = s(0)\exp(\lambda\, t)$. For $\epsilon = 10^{-5}$ we can infer from (figure 14,right) a value of $\mu = 3.5\,10^{-11}$. We have repeated the computation of μ for different values of ϵ up to $\epsilon = 10^{-3}$, i.e. close to the thresholds for diffusion on Λ but still below this thresholds. We report in figure 15 the comparison with the diffusion coefficient computed as reported in figure 3. With respect to figure 3 we have added the diffusion coefficient computed on a set of $N = 100$ initial conditions near $I_2 = 0.8$, i.e. in the same domain used for computing $d(s)$. The geometrical diffusion coefficient shows a remarkable agreement with the spread of orbits in the I_2 direction quantified by D. Although we are aware that this result is based on the detection of finite pieces of the unstable manifolds, the agreement with the diffusion coefficient on individual orbits confirms that the spread of the manifolds is significant to explain the diffusion that we detected numerically in section 2.

7 Conclusions

In this paper we have numerically detected the topology of the hyperbolic manifolds supporting diffusion in the a priori unstable dynamical systems using also new numerical methods. We find that the topology is correlated to the diffusion properties of the system. Precisely, we measured a spread of the asymptotic manifolds which is significant to explain diffusion. We also have shown that the stable and unstable manifolds have a topological transition when the Melnikov approximation looses its accuracy. This transition is correlated to a change of the law of dependence of the diffusion coefficient on the perturbing parameter. This suggests that the Melnikov approximation is not only a technical tool which allows one to compute accurate approximations

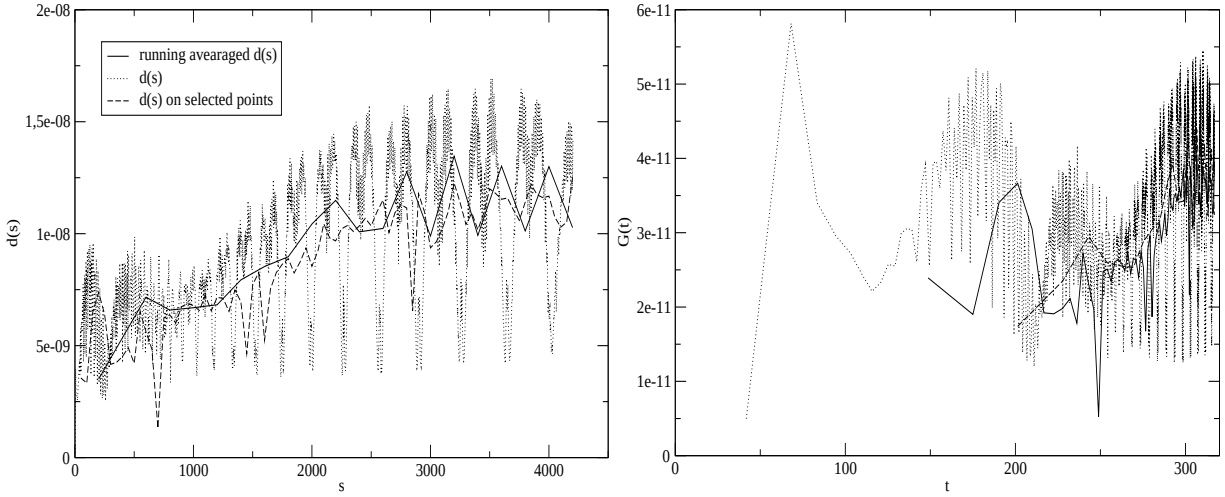

Figure 14: **On the left:** plot of $d(s)$ versus s for $\epsilon = 10^{-5}$ ($N = 200$, the initial conditions are $I_1 = 0$, $\varphi_1 = \pi$, $0.6 < I_2 < 1$, $\varphi_2 = 0$). The running average over a length $\Delta s = 200$ as well as the quantity $d(s)$ computed selecting the data with $|\varphi_1 - \pi| \leq 0.5$ are also plotted. **On the right:** plot of the quantity $G(t)$ defined in the text for the three data sets of left panel.

of the manifolds at small values of the perturbing parameters, but is related to a dynamical regime. The definition of a 'geometrical' diffusion coefficient and its comparison with the diffusion coefficient of orbits confirms the correlation among topology and diffusion.

8 Appendix: the Fast Lyapunov Indicator

A precise numerical detection of the dynamical character of an orbit is possible with the Fast Lyapunov Indicator whose definition is related to the Lyapunov exponent theory. In the numerical computations of the Lyapunov Characteristics Indicator (LCI hereafter) the attention is focused on the length of time necessary to get a reliable value of its limit, while very little importance is given to the first part of the computation. Actually, this part is usually considered as a kind of transitory regime depending, among other factors, on the choice of an initial vector of the tangent manifold.

In 1997, Froeschlé et al. [11] have remarked that the intermediate value of the largest LCI (which was called fast Lyapunov Indicator: FLI hereafter), taken at equal times for chaotic, even weakly chaotic, and ordered motions, allows one to distinguish between them. It turns

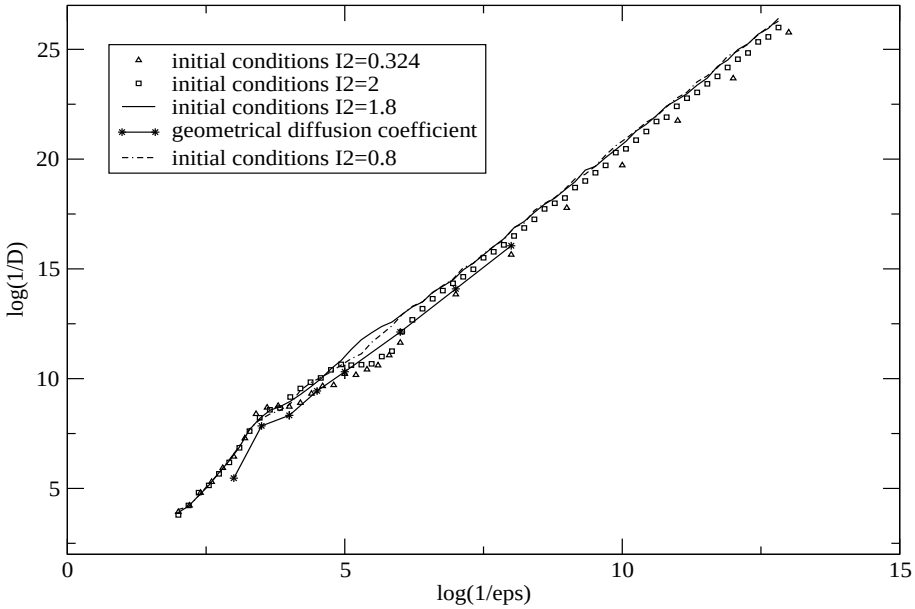

Figure 15: Variation of the diffusion coefficient as a function of ϵ for four sets of $N = 100$ initial conditions. The geometrical diffusion coefficient μ defined in the test shows a remarkable agreement with the spread of particles in the I_2 direction quantified by D.

out that the FLI allows also to distinguish among ordered motions of different origins, like resonant and non resonant motions [14]. This is not possible with the LCI, which tends to zero when t goes to infinity in both cases.

Given a map ϕ from $\mathbb{R}^n$ to $\mathbb{R}^n$, an initial condition $x(0) \in \mathbb{R}^n$, and an initial vector $v(0) \in \mathbb{R}^n$ of norm one, let us define the FLI function $FLI(x(0), v(0), T)$, $T > 0$, as:

$$FLI(x(0), v(0), T) = \sup_{0<t\leq T} \log ||v(t)|| \,, \tag{18}$$

where $v(t)$ is given by the system:

$$\left\{ \begin{array}{lcl} x(t+1) & = & \phi(x(t)) \\ v(t+1) & = & \frac{\partial \phi}{\partial x}(x(t))\, v(t) \,. \end{array} \right. \tag{19}$$

The definition trivially extends to continuous flows. In the specific case of quasi-integrable Hamiltonian systems:

$$H_\epsilon(I, \varphi) = h(I) + \epsilon f(I, \varphi) \quad , \tag{20}$$

for any initial condition $(I(0), \varphi(0))$ and any initial tangent vector $(v_I(0), v_\varphi(0))$, the FLI at time t is:

$$\log \|(v_I(t), v_\varphi(t))\| \quad . \tag{21}$$

In order to kill non significant fluctuations of (21), in formula (18) we have considered the supremum of the logarithm of the norm of the tangent vector. A running average could also have been used. Actually, as far as the mathematical development is concerned, we drop these averaging procedures, which however are useful in numerical computations. For $\epsilon = 0$ it is evidently:

$$v_I^0(t) = v_I(0) \quad , \quad v_\varphi^0(t) = v_\varphi(0) + \frac{\partial^2 h}{\partial^2 I}(I(0)) v_I(0) t \quad .$$

If ϵ is small we can estimate the evolution of $||v||$ with Hamiltonian perturbation theory. Following [14], if the initial condition is on a KAM torus then the norm $||v^\epsilon(t)||$ satisfies:

$$||v^\epsilon(t)|| = \left\| \frac{\partial^2 h}{\partial^2 I}(I(0)) v_I(0) \right\| t + \mathcal{O}(\epsilon^\alpha t) + \mathcal{O}(1) \quad , \tag{22}$$

with some $\alpha > 0$. As a consequence, the FLI has approximately the value of the unperturbed case on all KAM tori. Instead if the initial condition is on a regular resonant motion then it is [14]:

$$||v^\epsilon(t)|| = \|C_\Lambda \Pi_{\Lambda^{ort}} v_I(0)\|\, t + \mathcal{O}(\epsilon^\beta t) + t\mathcal{O}(\rho^2) + \mathcal{O}(\sqrt{\epsilon} t) + \mathcal{O}(\frac{1}{\sqrt{\epsilon}}) \tag{23}$$

with some $\beta > 0$, Λ^{ort} being the linear space orthogonal to an integer lattice Λ (the integer lattice $\Lambda \subseteq Z^n$ defines the resonance, see [14] for details), C_Λ is a linear operator depending on the resonant lattice Λ and on the initial action $I(0)$, $\Pi_{\Lambda^{ort}}$ denotes the projection over the lattice Λ^{ort}.

It is important to remark that the FLI on regular resonant motions is different at order $\mathcal{O}(1)$ from the unperturbed case on regular resonant motions. In fact, the linear operator $C_\Lambda \Pi_{\Lambda^{ort}}$ is different from the Hessian matrix of h at order $\mathcal{O}(1)$, i.e. $C_\Lambda \Pi_{\Lambda^{ort}}$ does not approach $\frac{\partial^2 h}{\partial I^2}$ as ϵ approaches to zero. In this way, we detect the presence of the resonances because the value of the FLI is different from the uniform value assumed on the KAM tori. Finally, for initial conditions on chaotic resonant motions the FLI is higher (since the tangent vectors growth exponentially with time) than the value characterizing KAM tori. As a consequence the resonance structure of the phase space can be detected computing the FLI with the same $v(0)$ and the same time interval t on a grid of regularly spaced initial conditions. The representation of the set of resonances of a quasi–integrable Hamiltonian system can be found in [12].

Acknowledgments. M. Guzzo has been supported by the project CPDA063945/06 of the University of Padova.

References

References

[1] Arnold V.I.: Instability of dynamical systems with several degrees of freedom. Sov. Math. Dokl., 6, 581–585, 1964.

[2] Guzzo, M., Lega E., Froeschlé C.: Hyperbolic manifolds supporting Arnold diffusion in quasi–integrable systems. Preprint, 2007.

[3] Hirsch M.W., Pugh C.C. and Shub M.: Invariant Manifolds. Lecture Notes in Mathematics, Vol. 583. Springer-Verlag, Berlin-New York, 1977.

[4] Chierchia L. and Gallavotti G.: Drift and diffusion in phase space. Ann. Inst. H.Poincaré, Vol. 60, 1–144, 1994.

[5] Bessi U., Chierchia L. and Valdinoci E.: Upper bounds on Arnold diffusion times via Mather theory. J. Math. Pures Appl., Vol. 80, 105–129, 2001.

[6] Delshams A., de la Llave R. and Seara T.M.: A geometric mechanism for diffusion in Hamiltonian systems overcoming the large gap problem: heuristics and rigorous verification on a model. Mem. Amer. Math. Soc. 179, no. 844, 2006.

[7] Chirikov, B.V.: An universal instability of many dimensional oscillator system. Phys. Reports, 52:265, 1979.

[8] Efthymiopoulos, C.; Contopoulos, G.; Voglis, N.: Cantori, Islands and Asymptotic Curves in the Stickiness Region. Celestial Mechanics and Dynamical Astronomy, v. 73, Issue 1/4, 221-230, 1999.

[9] Hasselblatt B. and Pesin Y.: Partially hyperbolic dynamical systems. Handbook of dynamical systems. Vol. 1B, 1–55, Elsevier B. V., Amsterdam, 2006.

[10] Guzzo M.: A direct proof of the Nekhoroshev theorem for nearly integrable symplectic maps. Annales Henry Poincaré, vol. 5, n. 6, 1013-1039, 2004.

[11] Froeschlé C., Lega E. and Gonczi R.: Fast Lyapunov indicators. Application to asteroidal motion. Celest. Mech. and Dynam. Astron., Vol. 67, 41–62, 1997.

[12] Froeschlé C., Guzzo M. and Lega E.: "Graphical Evolution of the Arnold Web: From Order to Chaos". Science, Volume 289, n. 5487, 2000.

[13] Froeschlé C., Lega E.: On the Structure of Symplectic Mappings. The Fast Lyapunov Indicator: a Very Sensitive Tool, Celestial Mechanics and Dynamical Astronomy, 78, Issue 1/4, p. 167-195, 2000.

[14] Guzzo M., Lega E. and Froeschlé C.: On the numerical detection of the effective stability of chaotic motions in quasi-integrable systems. Physica D, Volume 163, Issues 1-2, 1-25, 2002.

[15] Lega E., Guzzo M. and Froeschlé C.: "Detection of Arnold diffusion in Hamiltonian systems". Physica D, vol. 182, p. 179–187, 2003.

[16] Lega E., Froeschlé C. and Guzzo M.: "Diffusion in Hamiltonian quasi–integrable systems." In Lecture Notes in Physics, "Topics in gravitational dynamics", Benest, Froeschlé, Lega eds., Spinger. In press, 2007.

[17] Guzzo M., Lega E. and Froeschlé C.: "First Numerical Evidence of Arnold diffusion in quasi–integrable systems". DCDS B, vol. 5, n. 3, 2005.

[18] Froeschlé C., Guzzo M. and Lega E.: "Local and global diffusion along resonant lines in discrete quasi–integrable dynamical systems", Celestial Mechanics and Dynamical Astronomy, vol. 92, n. 1-3, 243-255, 2005.

[19] Guzzo M., Lega E. and Froeschlé C.: Diffusion and stability in perturbed non-convex integrable systems. Nonlinearity, **19**, pp 1049–1067, (2006).

[20] Mather J.N.: Arnold diffusion, I: announcement of results. Contemporary Mathematics and its Applications, Fundamental Directions April–May 2003 (Russian transl.), original to appear in J. Math. Sci.

[21] Treschev D.: Trajectories in a neighbourhood of asymptotic surfaces of a priori unstable Hamiltonian systems. Nonlinearity 15 2033-2052, 2002.

[22] Treschev D.: Evolution of slow variables in a priori unstable Hamiltonian systems. Nonlinearity 17 1803-1841, 2004.

[23] Simo C.: On the analytical and numerical approximation of invariant manifolds, in Modern Methods in Celestial Mechanics, D. Benest, Cl. Froeschlé eds, Editions Frontières, 285-329, 1989.

[24] Krauskopf, B., Osinga, H.M., Doedel, E.J., Henderson, enheimer, J., Vladimirsky, A., Dellnitz, M., Junge, O.: A survey of methods for computing (un)stable manifolds of vector fields. Int. J. Bif. and Chaos, **15**, 763-791, 2005.

[25] MacKay R.S.,Meiss J.D. and Percival I.C.: Transport in Hamiltonian Systems. Physica D, 13, 55–81, 1984.

[26] Broer H.W., Osinga H.M. and Vegter G.: Algorithms for computing normally hyperbolic invariant manifolds. ZAMP **48**, 480-524, 1997.